Low-temperature heat-capacity measurements of ^{4}He films adsorbed on a disordered substrate

Richard H. Tait* and John D. Reppy
Laboratory of Atomic and Solid State Physics and
Materials Science Center, Cornell University, Ithaca, New York 14853
(Received 15 December 1978)

The heat capacity of submonolayer, monolayer, and multilayer ^{4}He films adsorbed on a disordered substrate (porous Vycor glass) has been measured in the temperature range 0.08–1.3 K. Two distinct regions as a function of coverage were observed: (i) coverages less than 28.6 μmole m^{-2} (approximately 1.5 layers) and (ii) coverages greater than 28.6 μmole m^{-2}. Arguments are presented to show that for the low-coverage region the adsorbed helium forms a two-dimensional (2-D) solid with a small number of thermally activated adatoms moving in free-particle-like states on top of this solid layer. Arguments are also presented to show that for the high-coverage region a superfluid ^{4}He fraction lies on top of this initial 2-D solid below a transition temperature T_0. Measurements of the heat capacity of ^{4}He films adsorbed on N_2-preplated Vycor are presented to show that a precoating serves only to change the thickness of the 2-D solid layer and does not affect the form of the heat-capacity curves.

I. INTRODUCTION

In the past few years, considerable work has been carried out to measure the low-temperature ($T \lesssim 10$ K) properties of adsorbed helium films and to develop theoretical models to explain these measurements. Three areas of particular interest have been (i) the applicability of models of two-dimensional gases, two-dimensional liquids, and two-dimensional solids to monolayer and submonolayer ^{3}He and ^{4}He films[1–4]; (ii) the nature of the superfluid transition in multilayer ^{4}He films when the film thickness is only a few atomic layers[5–8]; and (iii) the nature of the excitation spectrum of superfluid ^{4}He in restricted geometries.[9–12]

In this paper we report on systematic measurements of the heat capacity of ^{4}He films (submonolayer, monolayer, and multilayer) adsorbed on a disordered substrate for the temperature range 0.08–1.3 K. This study was initiated to improve our understanding of the behavior of ^{4}He films adsorbed on disordered substrates as it is related to the three areas just mentioned.

In Sec. II of this paper we review the experimental and theoretical work on adsorbed helium films that pertains to the three problem areas of interest here. In Sec. III we describe the adsorbent used in this experiment and discuss the experimental techniques used to obtain the data. In Sec. IV we discuss our results and in Sec. V we summarize our findings and present our major conclusions.

II. BACKGROUND REVIEW

A. Monolayer and submonolayer films

The nature of the two-dimensional (2-D) single-particle states of adsorbed helium atoms on well-ordered surfaces has been the object of considerable theoretical work. Calculations have been made for He adsorbed on basal plane graphite[13,14]; Ar-plated copper[15]; Ar-,[16] Ne-[17] and Xe-plated[16] graphite; and the (100) face of LiF.[18] For all of these systems the calculations have shown that the single adatom states are free-particle-like in two dimensions so that in the limit of low densities the adsorbed He atoms would not be localized on atomic or molecular sites of the substrate at any temperature. Although no microscopic calculations have been made of the band structure of adsorbed He atoms on metallic surfaces, it is widely thought that the 2-D single-particle helium adatom states would be delocalized on these substrates as well.[15,19,20] Only for helium adsorbed on the open (100) faces of Ar and Kr have band-structure calculations shown indications for helium adatom localization.[21]

For the case of helium adsorbed on basal plane graphite, the adsorption potential is so smooth that the model calculations have indicated the substrate potential should have little effect on the properties of the adsorbed helium atoms other than to restrict their motion to two dimensions.[13,14,22] Measurements of the thermal properties of submonolayer and mono-

layer ^{3}He and ^{4}He films adsorbed on ordered basal plane graphite surfaces have amply confirmed this theoretical conclusion.[3,4] Excellent agreement has been obtained between the observed thermodynamic behavior of adsorbed helium films [in particular the low-temperature ($T < 4$ K) heat capacity] on graphite and the calculated thermodynamic behavior based on models of 2-D gases, liquids, and solids[3,4,23] that essentially ignored the presence of the substrate. Only for a few selected coverages does the graphite substrate play an active role. Based on these observations, a phase diagram has been proposed to describe helium films on this substrate[3] that satisfactorily accounts for the widely different behavior seen for different coverage regimes.[3,24,25]

While the low-temperature behavior of submonolayer and monolayer helium films on a well-ordered graphite surface is interpretable in terms of models of homogeneous 2-D phases, this is not the case for helium films adsorbed on disordered substrates. In particular, the low-temperature heat capacity of submonolayer and monolayer films on a wide variety of disordered substrates can all be fit by the same equation over a large temperature range; namely $C = AT + BT^2$, where A and B are substrate and coverage dependent parameters.[2,26–28] This equation fits data for coverages ranging from about 4.5 μmole m^{-2} (approximately $\frac{1}{3}$ atomic layer) to about 30 μmole (about 1.5 atomic layers). No evidence of the 2-D phase transitions seen for helium on graphite have been reported for films on disordered surfaces nor has any clear evidence for 2-D gas or liquid behavior been seen.

To date, no completely satisfactory theoretical explanation of the behavior of low-coverage helium films on disordered substrates has been presented although it is now generally assumed that long-range variations in the adsorption potential of the substrate are ultimately responsible for these observed effects.[3,29] Roy and Halsey[29] have put forward the most successful model based on this assumption. They proposed that long-range adsorption potential variations exist on all disordered substrates and that these variations cause islands of helium to form. In this model the heat-capacity term linear in temperature arises from single-particle excitation of atoms out of the islands into higher energy states and the term quadratic in temperature comes from pseudo-Debye, 2-D vibrations of the islands. While offering a reasonable explanation for the generality of the observed behavior these authors did not address the problem of the nature of the single-particle states.[29]

B. Onset of superfluidity in thin ^{4}He films

The onset of superfluidity in thin ^{4}He films adsorbed on a number of different substrates has been studied with a variety of transport techniques including third sound,[30,31] persistent current,[32] pressure driven mass flow,[33] heat transport,[34] oscillating cavity,[8] and quartz oscillator frequency shift measurements.[35,36] From these experiments two general observations have been made concerning the behavior of the onset temperature T_{onset} and the superfluid mass M_s (measured near $T = 0$) as a function of film thickness d: (i) $T_{onset} \to 0$ as $d \to d_0$,[8,32] and (ii) $M_s \to 0$ as $d \to d_0$.[8,30–32,35] Here d_0 is an experimentally determined film thickness that has been found for a number of different substrates to be about 1.3 to 1.5 standard atomic layers.

While much experimental work has been carried out, this observed behavior is only partially understood at present. The characteristic thickness d_0 is now generally regarded as being composed of a solid layer next to the substrate surface and only the extra helium on top of this solid layer is thought to be fluid and to participate in superflow.[37] There have been attempts to describe the form of the onset curve for thicker films ($d > 2$ layers) in terms of the temperature-dependent healing length theory of Ginzburg-Pitaevstii,[38] a model Ginzburg-Landau model field theory,[39] and percolation theories.[40,41] Finally, models of interacting vortex pairs[42] have been used to describe the decay of superfluidity in two-dimensional superfluid systems.[43,44]

C. Elementary excitations of superfluid ^{4}He in restricted geometries

The excitation spectrum of superfluid ^{4}He films of reduced dimensionality has been studied both experimentally and theoretically. In particular, third sound,[30] fourth sound,[45] U-tube,[10] persistent current,[46] and oscillating cavity[11] techniques have been used to measure the temperature dependence of the superfluid density of He II in restricted geometries utilizing a variety of substrates including Ar,[30] porous Vycor glass,[11,45] and packed powders.[10] Furthermore, specific-heat measurements have been carried out at moderately low temperatures ($T > 0.5$ K) for superfluid ^{4}He films adsorbed on basal plane graphite[47] and porous Vycor glass.[2,9] Theoretically, the excitation spectrum of superfluid helium of reduced dimensionality has been calculated for a number of model geometries utilizing various quantum hydrodynamic approaches[12,48] as well as variational calculation techniques.[49] The experimental measurements have led to three general conclusions: (i) the roton energy gap for adsorbed superfluid films is lower than the bulk value ($\Delta_{bulk}/k_B = 8.7$ K) by as much as 30% to 40%[9,11]; (ii) films having a gas-liquid interface have a large number of surface modes (ripplons or third sound waves) that are associated with the gas-liquid interface and give rise to a

large normal fluid density[8,9,31]; and (iii) superfluid films filling porous materials (i.e., with no gas-liquid interface) also have considerably higher normal fluid densities ρ_n than bulk He II.[10,11,46]

Theoretical calculations of the roton portion of the excitation spectrum have been limited. Padmore has calculated the roton portion of the spectrum for two-dimensional rotons and found that the calculated value of the roton energy gap for the two-dimensional system was about 2 K less than the calculated roton energy gap for bulk He II.[49]

On the other hand, the long-wavelength dispersion relation for vibrational excitations of He II in restricted geometries has been studied theoretically by a number of people using quantum hydrodynamic models. In particular, Saam and Cole[12] have developed a very general quantum hydrodynamic theory of these excitations that can be applied to any geometry and can be shown to include previous theories as special cases. This hydrodynamic theory has been applied to thin films having gas-liquid interfaces in an attempt to describe the quantized surface vibrational modes (ripplons or third sound waves) which have been so extensively studied experimentally. This theory has also been applied to thin films without a free surface in an attempt to explain the presence of excess bulk phonon modes (fourth sound waves) that have been observed.[45,48] Good agreement between predicted and measured dispersion relations has been found for third sound waves in planar geometries. However, while this theory has helped to clarify the role of size effects and substrate geometry in determining the excitation spectrum for more complicated geometries, detailed agreement between theory and experiment on the absolute magnitude of the number of excess excitations has not been provided.[48,52]

III. EXPERIMENTAL DETAILS

A. Substrate mounting

The adsorbent used in the helium film experiments reported here was a rod-shaped piece of porous Vycor glass (Corning code 7930) which was 1.07 cm in diameter and 2.40 cm in length. This porous material was made from a sodium borosilicate glass that had spinoidally decomposed into two interpenetrating phases: (i) a sodium-borate-rich phase and (ii) a silica-rich phase. The sodium-borate-rich phase was leached out with acid to leave a set of interconnected channels. The remaining solid material was 96% SiO_2.[50]

The sample of porous glass was mounted in the following manner. First, a thin walled, cylindrical chamber (open at one end) was machined from a cylindrical piece of hardened Stycast 1266 epoxy. Six strips of thin copper foil (2.70 cm long ×0.29 cm wide ×0.0013 cm thick) were then attached lengthwise to the exterior of the as-received piece of Vycor with GE7031 varnish. Next the piece of Vycor was inserted into the epoxy chamber with the long ends of the strips of copper foil protruding from the open end. The open end of the chamber, the bottom of the Vycor sample and the ends of the copper strips were then cast into another piece of epoxy. This bottom piece of epoxy served to seal the chamber and to physically connect the Vycor and copper strips to it.

After the epoxy had cured, a small hole was drilled into the opposite end of the vessel and a small Cu-Ni capillary (0.025 cm i.d. ×0.040 cm o.d.) was inserted into it. The capillary was sealed into the chamber with more Stycast 1266. A carbon resistance thermometer (constructed from the resistive element of speer 220-Ω, $\frac{1}{2}$-W resistor) was then attached to the Stycast chamber with GE7031 varnish. A 1000-Ω Nichrome wire heater was wound around the exterior of the chamber and was also attached with GE7031 varnish.

The vessel was placed in a brass mount where it was supported between nylon pins. This brass holder was bolted to a copper support which was connected to the mixing chamber of a dilution refrigerator. A 20 cm length of 0.0055 cm diameter copper wire was used as a thermal link between the sample chamber and the brass mount. The entire sample and sample chamber configuration is shown in Fig. 1.

The Cu-Ni capillary coming out of the epoxy vessel was soldered into the center section of a copper Tee joint. One side of the Tee led to a Cu-Ni capillary (0.010 cm i.d. ×0.080 cm o.d.) that went to the

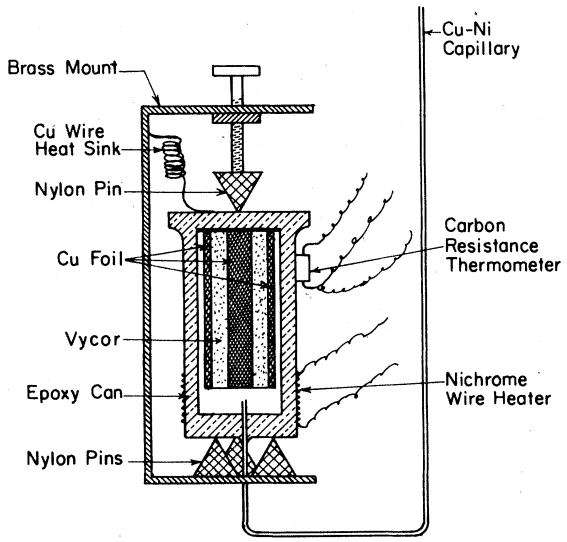

FIG. 1. Vycor sample and Vycor sample chamber configuration.

room-temperature gas handling system. The other side of the Tee led to a 15 cm length of copper tubing (0.31 cm i.d. ×0.63 cm o.d.). A liquid-nitrogen trapped diffusion pump was attached to this large diameter tubing and was used to pump on the vessel containing the Vycor substrate.

To clean the Vycor sample before cooling to low temperatures it was first flushed with ^{4}He gas at room temperature and then evacuated with the diffusion pump for 24 hours. To seal off this pump-out line the copper tubing was pinched shut (while still evacuated) and soldered over. Following pinchoff, a vacuum can was attached around the refrigerator-sample assembly. The can was then evacuated and inserted into a Dewar in preparation for cool down.

The piece of Vycor was mounted in as-received condition, i.e., no effort was made to drive off adsorbed gases prior to sealing the sample into the epoxy chamber. The only cleaning procedure used on the adsorbent was the room-temperature flush and pump previously mentioned. However, analysis of the heat-capacity data to be presented later (in particular comparison of the present data with the data of the Sussex group for ^{4}He on Vycor) demonstrates that for porous Vycor glass the cleanliness of the surface prior to adsorption of ^{4}He does not have a critical effect on the *form of* the heat-capacity curves.

B. Gas-handling techniques

Gas doses were metered into the sample chamber from a small (70.9 cm^3) dosing volume. Before each dose, this small volume was filled from a larger volume (1040.0 cm^3) that had previously been filled with purified ^{4}He. Gas pressure measurements were made with a capacitance manometer and were accurate to ±0.05 Torr. Total helium coverages were known to better than 0.3%.

For the preparation of an adsorbed helium film the following procedure was used: (i) the valve joining the room-temperature gas-handling system to the low-temperature sample chamber was opened and gas was admitted to the chamber, (ii) heat was applied to the sample chamber to raise its temperature to a preselected value for annealing while the valve was still open, (iii) the porous Vycor was allowed to stand at this annealing temperature for approximately one hour before heat to the sample was turned off, (iv) the chamber was allowed to cool to $T = 1.8$ K overnight with the valve to the gas-handling system still open, and (v) the valve was closed and the sample chamber was cooled to the desired temperature for heat-capacity measurements. No exchange gas was used in the vacuum can during helium adsorption. Coverages less than 26 μmole m^{-2} were annealed to 9 K or higher and coverages greater than 26 μmole m^{-2} were annealed to 4 K or higher.

N_2 adsorption measurements for the determination of surface area were carried out in a different cryostat. In this cryostat ^{4}He gas was admitted into the vacuum can to act as exchange gas and the can was immersed directly into a liquid N_2 bath. The same room-temperature gas-handling system was used for the N_2 adsorption experiments as was used for the ^{4}He adsorption work.

For the experiments utilizing a preadsorbed layer of N_2 on the porous Vycor, the sample chamber was cooled below $T = 77$ K prior to filling the Dewar with liquid helium in order to lower the vapor pressure of the adsorbed nitrogen so as to insure that no solid nitrogen block would form in the small diameter gas dosing lines. This precooling was accomplished by filling the Dewar with liquid nitrogen and pumping it away before transferring liquid ^{4}He.

C. Substrate characterization

A nitrogen adsorption isotherm at $T = 77$ K was measured for our sample of porous Vycor. The isotherm is shown in Fig. 2. Analysis of the adsorption data using the BET (Brunauer-Emmett-Teller) equation[51] yielded a surface area $A = 301$ m^2 assuming an area of 16.2 Å^2 for the nitrogen molecule. A total of 394 cm^3 NTP of N_2 was required to fill the pores indicating an open volume $V_{\text{open}} = 0.607$ cm^3. Assuming the open volume to be composed of identical, nonintersecting cylindrical pores we find the volumetric pore radius to be $r_p = 40.3$ Å.

The hysteresis in the adsorption-desorption isotherm is characteristic of porous media and can be explained in terms of capillary condensation and the existence of a pore size distribution in the material. Using the "ink-bottle" model for the pores shown in Fig. 3 we can calculate (using the Kelvin equation to describe the capillary condensation) the value of r_2 from the adsorption isotherm and the value of r_1 from the desorption isotherm.[51] After correction for the thickness of the adsorbed film on the surface we find that $r_1 = 32$ Å and $r_2 = 52$ Å.

The amount of ^{4}He required to fill the pores at $T = 1.2$ K was found using a capacitance technique suggested by M. Chan.[52] A capacitor composed of large pore filter paper pressed between copper screen electrodes was enclosed in an epoxy chamber that was connected to the Vycor sample chamber. ^{4}He gas was dosed in and the capacitance of the filter paper capacitor was measured with a General Radio Model 1615A capacitance bridge following each dose. The results are shown in Fig. 4. As long as the pores of the Vycor are not full only a thin film of helium forms on the filter paper and the capacitance does not change appreciably. However, after the pores of the Vycor are full the larger pores of the filter paper fill quickly and the capacitance rises sharply. After

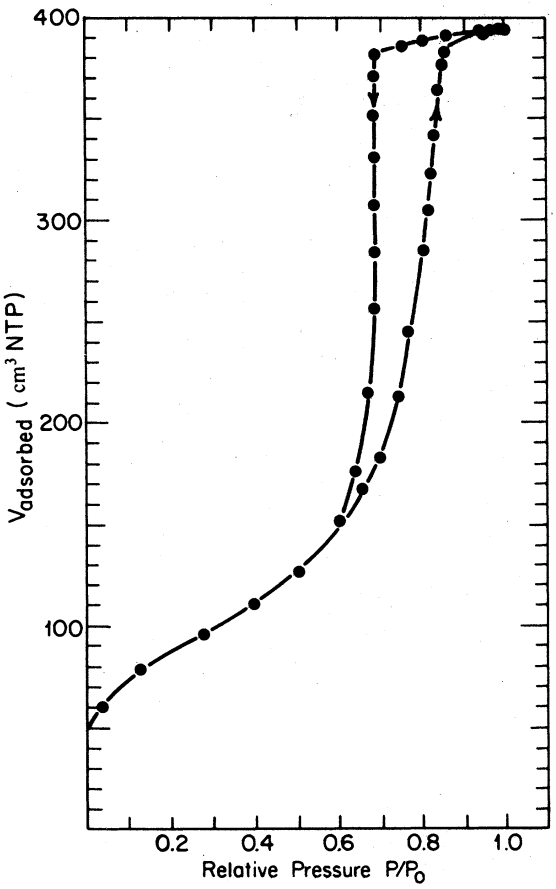

FIG. 2. N_2 adsorption-desorption isotherm for porous Vycor sample used in this study. P_0 is the saturated vapor pressure at $T=77$ K.

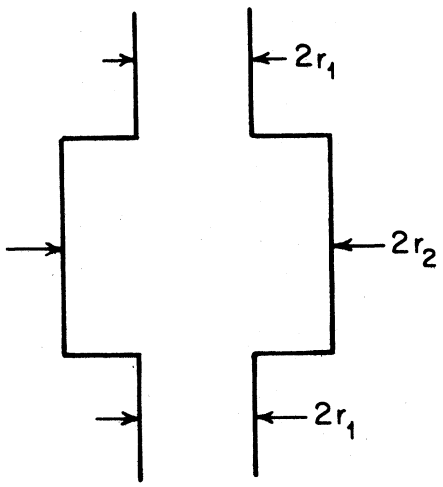

FIG. 3. "Ink-bottle" model of the pores in porous Vycor glass. Calculations using the Kelvin equation and the adsorption-desorption isotherm from our sample indicate that $r_1=32$ Å and $r_2=52$ Å.

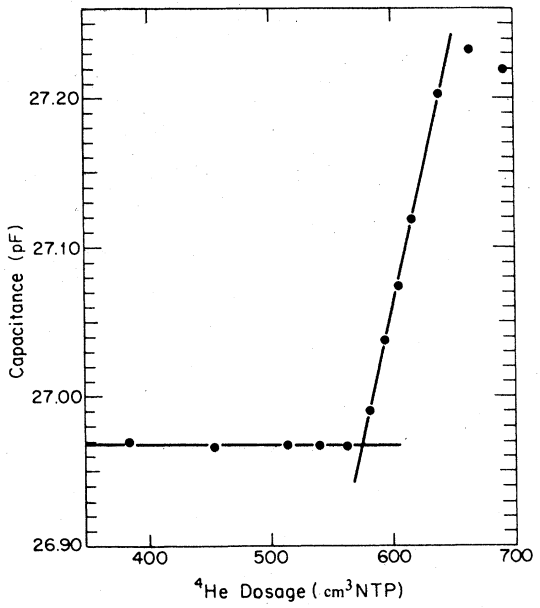

FIG. 4. Capacitance of filter paper capacitor in parallel with our porous Vycor sample as ^{4}He is adsorbed at $T=1.2$ K. Sharp rise beginning at $V_{adsorbed}=572$ cm^3 NTP indicates porous Vycor sample is full.

correction for helium adsorbed on the filter paper we find that the amount of ^{4}He required to fill the pores was $N_{full}=572$ cm^3 NTP (0.0255 moles). The characteristics of the sample used in this study are summarized in Table I.

Because we plan to make extensive reference to the specific-heat measurements made at the Univ. of Sussex[2] and the superfluid measurements of Berthold *et al.*,[8] we include the N_2 adsorption isotherms for the Vycor samples used in these experiments.[53,54] In Fig. 5 we plot the N_2 adsorption isotherm (at $T=77$ K) of all three samples of porous Vycor. We have normalized the data to the BET surface area of each sample. As is readily apparent, the three isotherms are in quantitative agreement for $P/P_0 \leq 0.6$. We take this equivalence as strong evidence that these three pieces of Vycor also have equivalent adsorption properties for helium at low and intermediate coverages. We therefore argue that helium films of equal surface density (measured in μmole m^{-2}) on all three substrates should have comparable properties.

Coverages in this paper will be given in two units: (i) fractional filling θ (the amount of helium adsorbed divided by the total amount of helium required to fill the pores) and (ii) surface density (μmole m^{-2}). The thickness of the film in Å or standard layers (one standard layer $\equiv 3.6$ Å) will in general not be given in this paper because this linear dimension is not a well-defined quantity for helium ad-

TABLE I. Parameters describing the sample of porous Vycor glass used in the present experiments.

Surface area	Open volume	Amount of ^{4}He to fill pores	Volumetric pore radius	Maximum pore radius	Minimum pore radius
301 m^2	0.607 cm^3	572 cm^3 NTP (0.0255 mole)	40.3 Å	52 Å	32 Å

sorbed on porous Vycor. Only in a few selected instances will an approximate film thickness be assigned. At low coverages ($\lesssim 20$ μmole m^{-2}) the films will not be uniform in thickness due to the large heterogeneous adsorption potential so that an assignment of a film thickness is not appropriate. At high coverages ($\gtrsim 40$ μmole m^{-2}) the film thickness is effected by the finite radius of the pores and the distribution of pore radii. This finite radius effect causes capillary condensation as well as giving rise to a film thickness that is not a linear function of coverage so that again a film "thickness" is not well defined. However, in order to facilitate comparison of the present data with the data of other researchers we do note that based on the ^{4}He adsorption isotherms of Symonds[54] and using the Van der Waals constant of $\Gamma = 27$ layer K^{-1} for glass[55] a coverage of 29 μmole m^{-2} corresponds to a film thickness of 1.5 standard atomic layers.

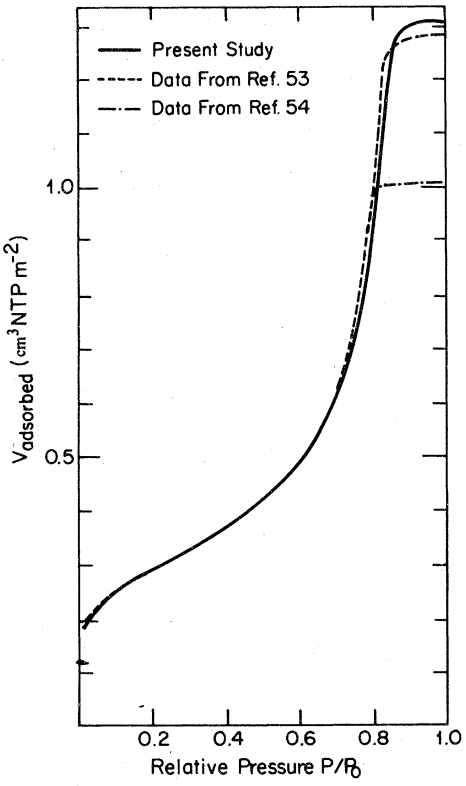

FIG. 5. N_2 adsorption isotherms (normalized to unit surface area) for different samples of porous Vycor glass. Data for sample used at the University of Sussex from Ref. 54 and data for sample used by Berthold and co-workers from Ref. 53.

D. Thermometry

As mentioned earlier, temperature measurements were made with a carbon resistance thermometer that had been constructed from the resistive element of a Speer 220-Ω, $\frac{1}{2}$-W resistor. The thermometer was cycled several times between room temperature and helium temperature before being used in the specific-heat experiments reported here. This thermometer was calibrated both before and after the specific-heat measurements using a precalibrated Cryo-Cal Ge resistance thermometer as a standard. The two calibration curves of the carbon heat-capacity thermometer differed less than 1% over the entire temperature range.

E. Heat-capacity measurements

Heat-capacity measurements were made using the standard technique of observing the change in resistance of a calibrated resistance thermometer attached to the sample can following the application of a short ($\Delta t \sim 2$ sec) heat pulse. A 33-Hz, ac resistance bridge coupled to a PAR 120 lock-in detector was used to measure the thermometer resistance. A typical response curve is shown in Fig. 6.

The observed overshoot at short times following the application of the heat pulse is due to the sample coming to internal equilibrium. In the example shown in Fig. 6, the heat leaks into the porous Vycor sample from the sample can with a time constant of about 5 seconds. The long time constant ($t = 300$ sec) exponential decay of the sample temperature is due to heat leaking out of the sample through the weak thermal link to the dilution refrigerator. The change in temperature ΔT due to the heat pulse was determined by extrapolating the exponential decay of ΔR back to $t = 0$ and converting this value of ΔR into an appropriate ΔT using the predetermined R vs T calibration curve.

The raw data was then corrected to take into account two important effects: (i) the more rapid loss

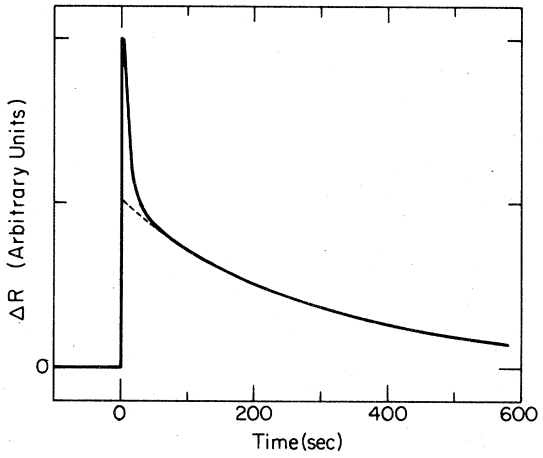

FIG. 6. Typical resistance thermometer response following a short (2 sec) heat pulse at time $t=0$. Solid line is observed response and dotted line is extrapolation of long time ($t > 50$ sec) behavior back to $t=0$.

of heat from the sample that took place during the initial overshort and (ii) the heat loss due to desorption of gas from the porous Vycor sample. Evaluation of the heat lost during the initial overshort was made using the measured temperature profile and the measured thermal conductance of the copper wire thermal link. This correction was always less than 7%.

The desorption contribution to the heat loss was estimated from the known volume of the sample can and the open volume of the Vycor sample using the ^{4}He adsorption isotherms for porous Vycor (properly scaled) measured by Symonds.[54] This correction was found to be 10% or less for all the data shown and less than 5% for data taken below $T=0.9$ K.

The maximum total error in the corrected heat-capacity points (errors due both to uncertainties in correction factors and experimental variations) was approximately ±10%.

IV. RESULTS AND DISCUSSION

A. Bare Vycor

Examination of the heat-capacity data for ^{4}He adsorbed on bare Vycor glass indicates that the nature of the adsorbed film varies markedly with coverage. Shown in Fig. 7 is the total ^{4}He heat capacity at $T=0.1$ K as a function of coverage. The large peak clearly divides the films into two distinct regions of coverage: (i) coverages with θ (fractional filling) < 0.337 (28.6 μmole m^{-2}) and (ii) coverages with $\theta > 0.337$ (28.6 μmole m^{-2}). As noted earlier (see Sec. II) a coverage of 29 μmole m^{-2} corresponds to a film thickness of about 1.5 standard atomic layers.

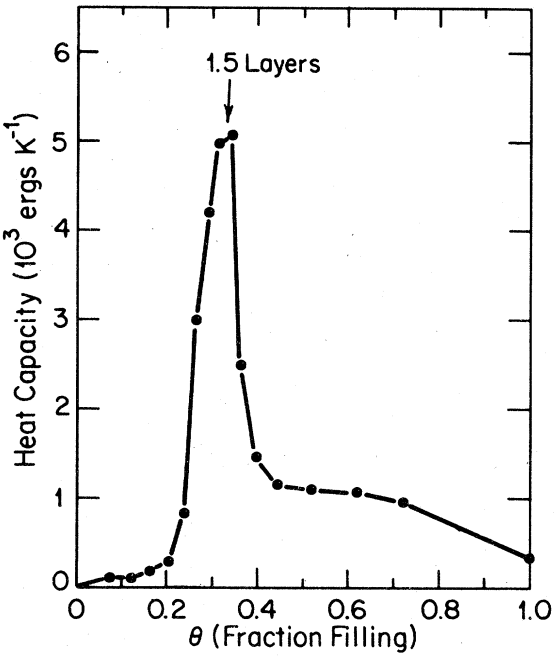

FIG. 7. ^{4}He heat capacity as a function of ^{4}He coverage at $T=0.1$ K.

In the rest of this section we will discuss in detail the heat-capacity data for ^{4}He adsorbed on bare Vycor. In particular we have separated the data into three overlapping coverage regimes. For each region we will discuss the observed behavior and give possible explanations for that behavior. The three regions are as follows: (i) coverages with $\theta \leq 0.319$ (27.1 μmole m^{-2}) (ii) coverages near the critical coverage $\theta=0.330$ (28.6 μmole m^{-2}) and (iii) coverages with $\theta > 0.397$ (33.7 μmole m^{-2}).

1. *Low-coverage films:* $\theta \leq 0.319$ (27.1 μmole m^{-2})

A representative set of heat-capacity curves for coverages in this group are shown in Fig. 8 along with the measured heat capacity of the empty calorimeter. As can be seen from the figure, the exact temperature dependence of the helium heat capacity varies with coverage. Close examination of the data indicates that the heat capacity of *all* coverages in this region can be reasonably well fit with two simple expressions which are suggested by model calculations to be discussed later. These expressions are as follows:

$$C = AT + BT^2, \quad T > T_c \tag{1}$$

and

$$C = D(\Delta/k_B T + 2)\, e^{\beta\Delta} + B'T^2, \quad T < T_c\,. \tag{2}$$

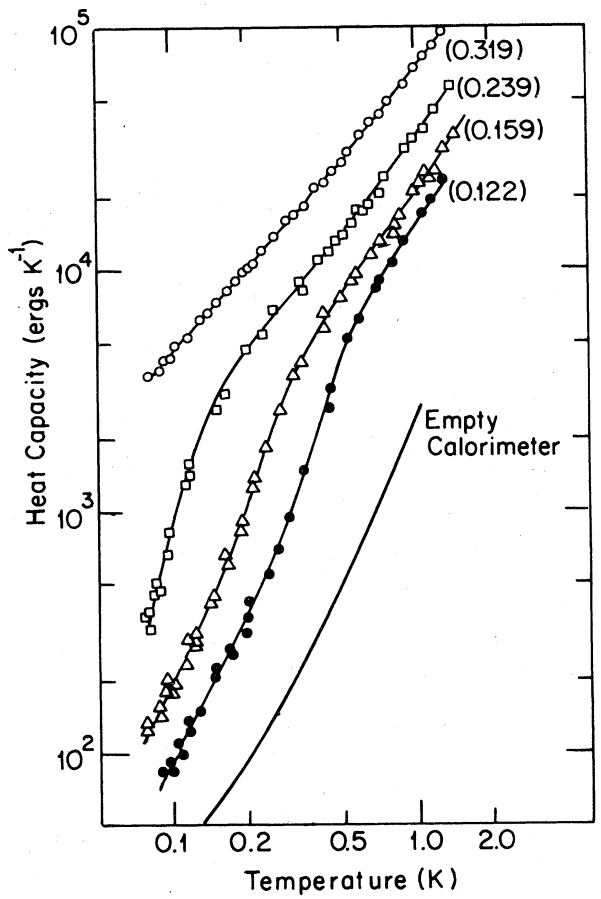

FIG. 8. ^{4}He heat capacity of a representative set of ^{4}He coverages on porous Vycor for $\theta \leq 0.319$ (27.1 μmole m^{-2}). Numbers in parentheses are ^{4}He coverages expressed as fractional filling of the pores. Solid lines are drawn as aid to the eye.

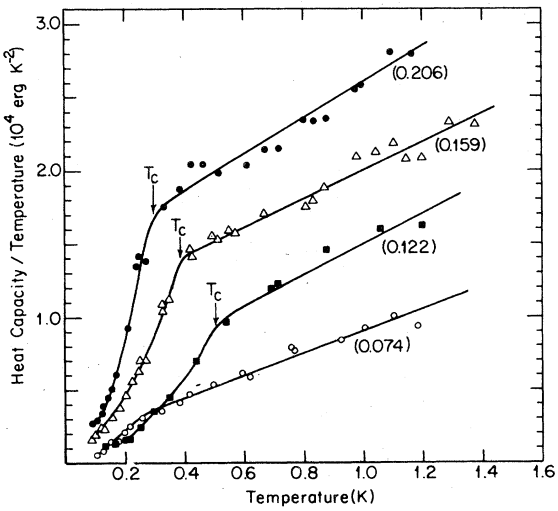

FIG. 9. ^{4}He heat capacity divided by temperature for the lowest coverages on porous Vycor. Numbers in parentheses are ^{4}He coverages expressed as fractional filling. Solid lines are fits to the data using Eqs. (1) and (2) (see text).

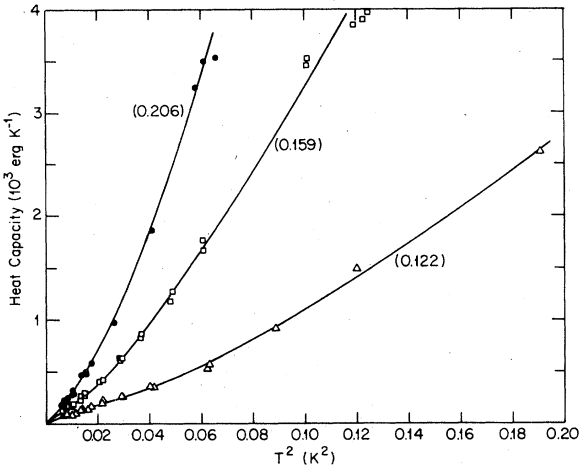

FIG. 10. ^{4}He heat capacity for three of the lowest coverages on porous Vycor. Data have been plotted vs T^2 to emphasize the T^2 dependence of the data at the lowest temperatures. Numbers in parentheses are ^{4}He coverages expressed as fractional filling. Solid lines are fits to the data using Eq. (2) (see text).

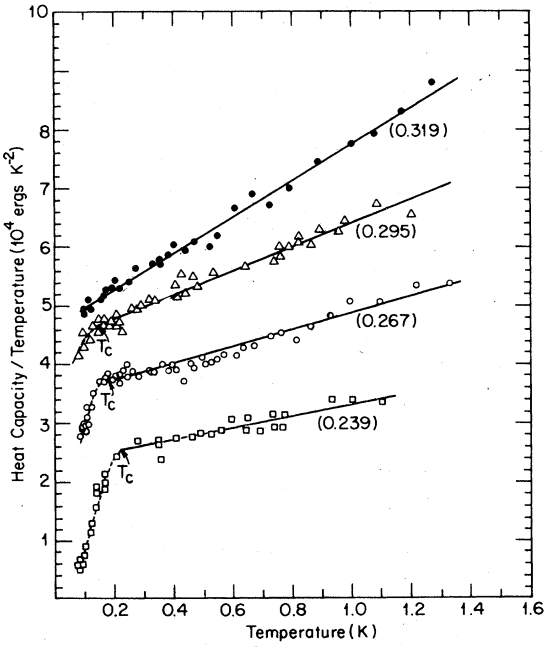

FIG. 11. ^{4}He heat capacity divided by temperature for intermediate coverages on porous Vycor. Numbers in parentheses are coverages expressed as fractional filling. Solid lines are fits to the data using Eq. (1) (see text). Dashed lines are drawn as an aid to the eye.

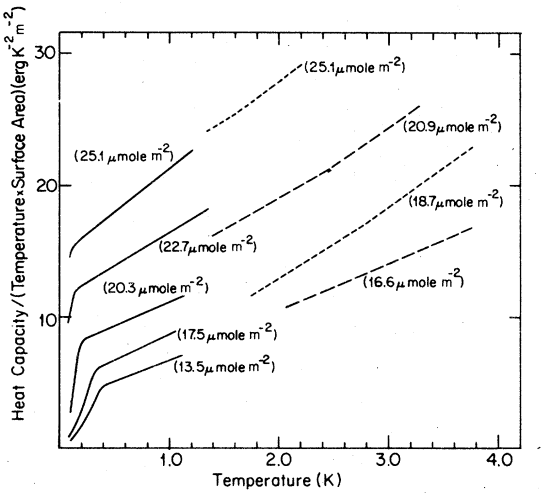

FIG. 12. ^{4}He heat capacity divided by temperature for low- and intermediate-coverage ^{4}He films on porous Vycor. Solid lines are from the present study and dashed lines are from Ref. 2. Numbers in parentheses are surface coverages.

Here T_c is a coverage dependent cutoff temperature that decreases smoothly as coverage increases. A, B, B', D, and Δ are coverage dependent parameters and $\beta \equiv 1/k_B T$.

The heat-capacity data for all coverages with $\theta \leq 0.319$ (27.1 μmole m^{-2}) are given in Figs. 9–11. In all three figures, the solid lines are fits to the data using Eqs. (1) and (2) with a smooth joint in the vicinity of $T = T_c$. The data have been plotted so as to emphasize the temperature dependences just mentioned. In Figs. 9 and 11 we have plotted C/T vs T to emphasize the high-temperature behavior described by Eq. (1). In Fig. 10 we have plotted C vs T^2 for the three lowest coverages to emphasize the T^2 dependence of Eq. (2).

In Fig. 12 we have plotted the heat-capacity data of the Sussex group[2] along with data from the present experiments. Both sets of data have been normalized to unit surface area. As can be seen, the agreement between the present work and the work of the Sussex group is fairly good for overlapping coverages and temperatures.

The agreement between the heat-capacity data and the fitting functions is satisfactory. Figures 9 and 11 demonstrate that the fit to the heat-capacity data above T_c utilizing Eq. (1) is quite good. Figure 12 shows that Eq. (1) fits the data up to $T = 3$ K. Examination of Fig. 11 shows that Eq. (2) describes the data reasonably well at low coverages for $T < T_c$. Because the temperature range used for the fit for Eq. (2) is quite small, a number of other functional forms could have been used to satisfactorily account for the data. Nevertheless the sharp drop in the heat capacity below T_c is most easily described with a term containing an exponential temperature dependence as in Eq. (2). In Table II we list the parameters that characterize the data for coverages with $\theta \leq 0.319$ (27.1 μmole m^{-2}).

The values for T_c shown in Table II are the temperatures at which the low-temperature fit intersects the high-temperature fit, i.e., the temperature for which the heat capacity given by Eq. (1) is equal to the heat capacity given by Eq. (2). As mentioned previously, the value of T_c decreases smoothly with coverage. This behavior is shown graphically in Fig. 13. As can be seen from Table II we find $T_c \sim \frac{1}{3}$ to $\frac{1}{4}$ of Δ/k_B.

To explain the behavior of ^{4}He films in this coverage regime semiquantitatively we propose the following simple model based on some of the suggestions of Roy and Halsey[29] and Daunt[56] concerning the nature of helium films adsorbed on heterogeneous surfaces. Following Roy and Halsey we argue that the fluctuations of the adsorption potential for helium atoms are not distributed randomly across the surface

TABLE II. Parameters used to fit low-coverage heat-capacity data using Eqs. (1) and (2).

θ (Fractional filling)	T_c (K)	A (10^4 erg K^{-2})	B (10^4 erg K^{-3})	Δ/k_B (K)	D (10^4 erg K^{-2})	B' (10^4 erg K^{-3})
0.074	. . .	0.15	0.77	. . .	. . .	. . .
0.122	0.50	0.42	1.08	1.9	1.3	0.83
0.159	0.38	1.10	0.96	1.25	1.2	1.9
0.206	0.32	1.36	1.26	1.0	1.7	2.7
0.239	0.22	2.33	0.98	. . .	. . .	. . .
0.267	0.13	3.42	1.42	. . .	. . .	. . .
0.295	0.08	4.35	2.07	. . .	. . .	. . .
0.319	. . .	4.65	3.10	. . .	. . .	. . .

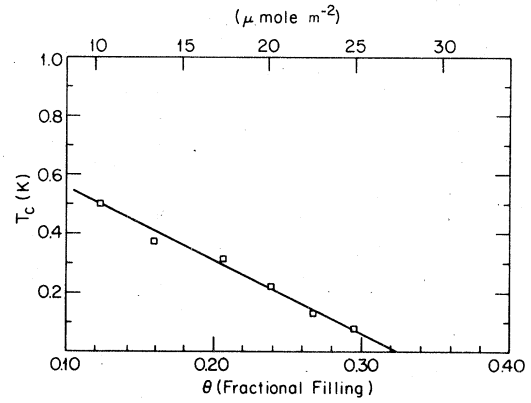

FIG. 13. Coverage dependence of the cutoff temperature T_c.

but are grouped together so as to give rise to long-range variations. The long-range variations in turn give rise to large lateral pressures on the adsorbed helium atoms at low coverage. Therefore, while the atomic potential due to the substrate is not strong enough to localize the helium adatoms on atomic or molecular sites, these large lateral pressures are sufficiently strong to force the helium atoms to form islands. Consequently, at $T=0$ the adsorbed helium consists solely of solid patches (possibly interconnected at sufficiently high coverage) of adatoms on the surface.

A schematic of the adsorption potential, which we propose is seen by the last helium atom adsorbed, is shown in Fig. 14. We also propose that an adsorption potential of this *form* is found for all coverages. Here we have proposed that the length scale of the variation of the adsorption potential is comparable to the Vycor pore radius. The energy U_0 is the total potential energy of adsorption and 2Δ is the magnitude of the variation across the surface. We expect that $U_0 >> \Delta$. The values of Δ and U_0 will change as the coverage changes, but we expect that Δ will change more slowly with increased coverage of helium than will U_0; i.e., we expect that $\Delta/U_0 \sim$ constant so that $d\Delta/dN_{\text{ads}} << dU_0/dN_{\text{ads}}$. Now in our model 2Δ is the barrier for excitation of the least strongly bound adatom out of its localized position in an island into a delocalized two-dimensional free-particle-like state. This barrier is essentially the activation barrier for surface diffusion. The heat capacity of the film now consists of two parts: (i) the heat capacity associated with excitation of single particles out of the adatom islands and (ii) the heat capacity of the adatom islands themselves. As we will show, the energy gap 2Δ is responsible for the existence of the rapid decrease in heat capacity below T_c as the single-particle excitations are rapidly frozen out.

We will now evaluate the contribution of single-particle excitations to the observed heat capacity at a given coverage with the simple noninteracting single-particle energy-level diagram shown in Fig. 15. This energy-level diagram is consistent with the adsorption model just discussed. Here we have assumed that we can describe the energies of all of the adsorbed particles at $T=0$ (when they are all bound in the solid) with a single-particle density of states that is determined by the variation of adsorption energy with amount adsorbed. The most weakly bound atom has energy E_0 and the most strongly bound atom has energy 0. We have also assumed that these noninteracting single-particle states have single occupancy. For convenience sake we have also assumed that $G(\epsilon) = G(E_0) = G_0$ since this assumption greatly simplified the calculations and since we expect that $G(\epsilon)$ varies only slightly in the energy range (E_0 to $E_0 - \Delta - k_B T$) which contributes to the observed heat capacity. We also assume that the density, H_0, of free-particle states (which can have multiple occupan-

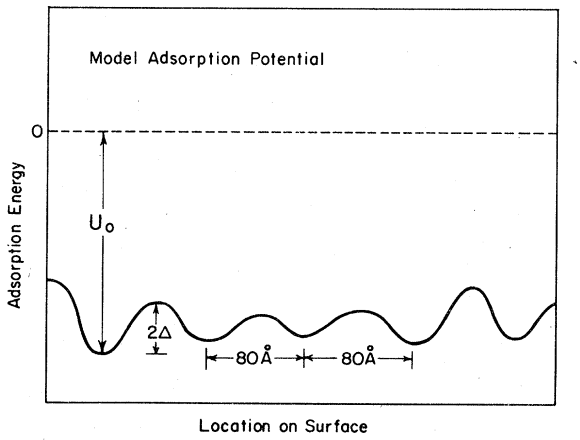

FIG. 14. Model spatial dependence of adsorption potential

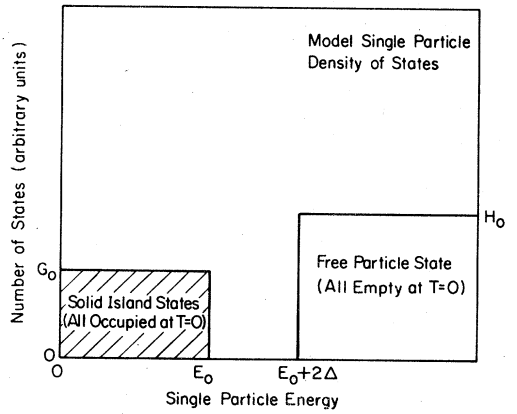

FIG. 15. Model single-particle density of states. Single occupancy for states below E_0 and multiple occupancy for states above $E_0+2\Delta$.

cy) which are present at energies greater than $E_0+2\Delta$ can be described by the density of states for the ideal 2-D gas which is a constant. The values of E_0 and G_0 will be coverage dependent.

Now for the case of $\Delta >> k_BT$ we find (see Appendix A) that the single-particle excitations give rise to a heat capacity C_{ex} given by

$$C_{ex}=2(G_0H_0)^{1/2}\Delta k_B\left(\frac{\Delta}{k_BT}+2\right)e^{\beta\Delta} . \tag{3}$$

In the opposite limit, $\Delta << k_BT$, we find (see Appendix A) that

$$C_{ex}=(K_1G_0k_B^2+K_2H_0k_B^2)\,T , \tag{4}$$

where K_1 and K_2 are constants of order unity.

To account for the portion of the heat capacity due to the adatom islands we follow Roy and Halsey[29] and propose that these islands behave like pseudo-Debye 2-D solids. Therefore they will contribute a term proportional to T^2 to the heat capacity. For a 2-D solid with transverse and longitudinal velocities of sound V_t and V_l respectively, we have

$$C_{\text{Debye}}=28.8Nk_B(T/\Theta_D)^2 , \tag{5}$$

where

$$\frac{1}{\Theta_D^2}=\left(\frac{k_B}{2\pi\hbar}\right)^2\frac{S}{N}\pi/2\left(\frac{2}{\nu_{\text{Debye}}^2}\right) \tag{6}$$

and

$$\frac{2}{\nu_{\text{Debye}}^2}\equiv\frac{1}{\nu_t^2}+\frac{1}{\nu_l^2} .$$

Here N is the number of adsorbed atoms and S is the total surface area. Combining Eq. (5) and Eqs. (3) and (4) we find

$$C_{\text{theor}}=(K_1G_0k_B^2+K_2H_0k_B^2)\,T +28.8Nk_B(T/\Theta_D)^2,\quad T>>\Delta/k_B , \tag{7}$$

$$C_{\text{theor}}=2(G_0H_0)^{1/2}\Delta k_B(\Delta/k_BT+2)e^{\beta\Delta} +28.8Nk_B(T/\Theta_D)^2,\quad T<<\Delta/k_B . \tag{8}$$

As can be readily seen, Eq. (7) is of the same form as the experimentally observed heat-capacity data described by Eq. (1) and Eq. (8) is of the same form as the experimentally observed heat-capacity data described by Eq. (2).

While our model has the correct temperature dependences, in order to demonstrate that it is reasonable we must show that the absolute magnitude of the theoretical heat capacity is in reasonable agreement with the magnitude of the experimentally observed heat capacity. We will carry out this comparison for the coverage $\theta=0.206$(17.5 μmole m^{-2}). In particular we will first determine reasonable values for the parameters G_0 and H_0. We will then use these values and the measured value of Δ to calculate the first term on the right side of Eqs. (7) and (8) and we will compare these calculated terms with the experimental values of the parameters A and D given in Table II. Next, we will calculate values for ν_{Debye} using Eqs. (5) and (6) and the measured values of the parameters B and B' given in Table II. We will then discuss the implication of the values for ν_{Debye}.

While we have no theoretical model to use to assign a value to G_0 we can make a reasonable approximation. Because we have assumed that the energies of the adsorbed adatoms are due to the variation of the adsorption potential with the amount of helium adsorbed, N_0, a reasonable estimate of $G(E_0)$ is

$$G(E_0)=\left(\frac{dQ_{\text{st}}}{dN_{\text{ads}}}\right)^{-1}_{N_{\text{ads}}=N_0} . \tag{9}$$

N_{ads} is the amount of helium adsorbed. Q_{st} is the isosteric heat of adsorption (in ergs/particle) which in the case of strongly heterogeneous surfaces is expected to be determined primarily by the variation of the adsorption potential with coverage rather than primarily by adatom-adatom interactions as in the case of homogeneous surfaces. While no measurements of the heat of adsorption for ^{4}He films on Vycor at low coverages have been made, we assume that a reasonable value for the variation of the adsorption potential for ^{4}He on glass for a coverage $\theta=0.206$ (17.5 μmole m^{-2}) is given by

$$G_0=2.2\times10^{35}\text{ states/erg}$$
$$=3.0\times10^{19}\text{ states/°K}$$

This value is a smooth extrapolation of higher-coverage data on Vycor[54] and is consistent with ^{4}He heats of adsorption measured on TiO_2,[57] Cu,[58] Ar-plated Cu.[58]

Now for the ideal 2-D Bose gas we have a constant density of states given by

$$H_{2D}(\epsilon)\equiv H_{2D}=\frac{m}{\hbar^2}\frac{S}{2\pi} . \tag{10}$$

Here S is the surface area available to the free particle and m is the mass of the particle. If all of our adsorbent area is available to the adsorbed ^{4}He atoms then we find

$$H_{2D}=2.88\times10^{36}\text{ states/erg}$$
$$=3.97\times10^{20}\text{ states/K} .$$

However, at this relatively low coverage only a fraction of the total surface area is probably available for the free-particle states due to the large variations of adsorption potential (see Fig. 14) which we believe are still present at a coverage of $\theta=0.206$ (17.5 μmole m^{-2}). We therefore choose the reasonable ap-

proximation that the free-particle density of states for ^{4}He on Vycor glass at this coverage is one third of the ideal two-dimensional density of states; i.e., we set

$$H_0 = 9.6\times10^{35} \text{ states/erg} .$$

Using the above values for G_0 and H_0 and the value of Δ for the coverage given in Table II [and after calculating the constants K_1 and K_2 using Eq. (A30) and Eq. (A31)] we find that

$$2(G_0H_0)^{1/2}\Delta k_B = 1.7\times10^4 \text{ erg K}^{-2}$$

and

$$K_1G_0k_B^2 + K_2H_0k_B^2 = 2.0\times10^4 \text{ erg K}^{-2} .$$

Comparison of these values with the values of D and A, respectively given in Table II for $\theta = 0.206$ shows satisfactory agreement.

The form of the variation of the experimental parameters A and D can be explained in our model by corresponding changes in the parameters H_0 and G_0. In particular, when coverage increases on Vycor both H_0 and G_0 increase as the strength of the adsorption potential (as measured by the isosteric heat of adsorption) weakens. Therefore A will also increase. However, as coverage increases Δ decreases so that the value of the parameter D need not necessarily increase as coverage increases. The coverage dependence of D will depend on the details of the coverage dependence of H_0, G_0, and Δ which our semiquantitative theory cannot hope to describe. Finally we note that the number of particles excited into free-particle states at $T = 1$ K (i.e., $N_{ex} \sim H_0k_BT = 1.3\times10^{20}$) is only a small fraction of the number of atoms adsorbed (i.e., $N_{ex}/N_{ads} = 0.04$) at $\theta = 0.206$ (17.5 μmole m^{-2}).

The fact that $B' \neq B$ for a coverage $\theta = 0.206$ (17.5 μmole m^{-2}) (see Table II) implies that the value of v_{Debye} is different above and below T_c if the pseudo-Debye model is valid to describe the T^2 terms in the heat-capacity data for this coverage. In particular we find [using Eqs. (5) and (6)] that

$$v_{Debye} = 3.6\times10^4 \text{ cm/sec}, \quad T > T_c$$

and

$$v_{Debye} = 2.5\times10^4 \text{ cm/sec}, \quad T < T_c .$$

TABLE III. 2-D Debye sound velocities for ^{4}He films on various substrates.

Substrate	Coverage (μmole m^{-2})	v_{Debye} (10^4 cm sec^{-1})	Reference
Graphite	13.7	2.27	3
Graphite	17.9	5.38	3
Ar-Plated Cu	12.1	3.37	27
Cu	12.1	3.89	26

These values of v_{Debye} are in the range of values of v_{Debye} found for submonolayer and monolayer ^{4}He coverages on Cu,[26] Ar-plated Cu,[27] and graphite.[3] (In Table III we show some of the values of v_{Debye} found for these other substrates.)

Now the reason that $v_{Debye}(T > T_c) > v_{Debye}(T < T_c)$ is not obvious. However, two possible explanations come readily to mind: (i) a pseudo-Debye 2-D solid is not a good model for the adsorbed film in one or both of the temperature regions or (ii) the nature of the vibrational excitations changes in going from one temperature region to the other. We do not accept the first explanation because there is too much evidence from other sources that low-coverage ^{4}He films form 2-D solid at low temperatures. Consequently we support the second explanation.

We argue that there is indeed a real difference between the density of phonon states responsible for the high-temperature T^2 term and the phonon density of states responsible for the low-temperature T^2 term. In particular we argue first that the spatial variations of the adsorption potential breakup the phonon spectrum into two parts: (i) $\lambda_{phonon} > 2d$ and (ii) $\lambda_{phonon} < 2d$. Here d is the size of the adatom islands and we assume $d = 80$ Å. Now the velocity of sound for vibrations within an island ($\lambda_{phonon} < 2d$) is determined by the strength of the ^{4}He-^{4}He interaction within the island which should be comparatively strong. However, the velocity of sound for elastic vibrations spanning more than one island ($\lambda_{phonon} > 2d$) should be determined by the strength of the adatom-island–adatom-island interaction which should be comparatively weak for low coverages when the islands should be only weakly connected. Therefore we should have

$$v_{Debye}(\lambda_{phonon} < 2d) > v_{Debye}(\lambda_{phonon} > 2d) .$$

Now we will estimate the temperature for which $\lambda_{phonon} > 2d$ and $\lambda_{phonon} < 2d$. Using $\omega = 2\pi v_{Debye}/\lambda_{phonon}$ and setting $\lambda_{phonon} = 2d = 160$ Å we find that

$$\omega_{phonon}(v_{Debye} = 3.6\times10^4 \text{ cm/sec}) = 1.42\times10^{11} \text{ sec}^{-1}$$

and

$$\omega_{phonon}(v_{Debye} = 2.5\times10^4 \text{ cm/sec}) = 0.99\times10^{11} \text{ sec}^{-1} .$$

Now in the dominant phonon approximation $\hbar\omega_{dom} = 2.6k_BT$ so that with

$$\omega_{phonon} = 1.42\times10^{11} \text{ sec}$$

we find $T_{phonon} = 0.41$ K and with

$$\omega_{phonon} = 0.99\times10^{11} \text{ sec}^{-1}$$

we find $T_{phonon} = 0.29$ K. Therefore for $T < 0.29$ K we should have $\lambda_{phonon} > 2d$ and for $T > 0.41$ K we should have $\lambda_{phonon} < 2d$. Now $T_c = 0.32$ which is in the middle of these two values. Therefore we find that our simple two-regime model works reasonably well in accounting for the observation of two values of ν_{Debye} for one coverage. However, our simple picture offers no avenue for calculating the absolute value of ν_{Debye} in the two regimes. In particular, such a calculation would require a knowledge of the strength of the island-island interaction, a quantity that is essentially impossible to estimate given the lack of detailed knowledge of the surface heterogeneity.

A number of thermodynamic studies of adsorbed ^{4}He on disordered substrates other than Vycor have shown behavior comparable to that reported here. The low-temperature heat-capacity data of Hickernell *et al.*[28] for ^{4}He films on copper can also be fit well by Eqs. (1) and (2) and the absolute magnitude of their data is comparable to ours. In particular, the change in the slope of the isosteric heat of absorption data for ^{4}He on copper as a function of coverage that occurs around 18 μmole m^{-2} (Ref. 59) correlates very well with the marked increase in the linear term in the heat capacity of the films observed near this coverage.[26,28] Also, the expectation that the heterogeneity of an annealed metal surface should be lower than that for a glass surface is born out by the observation that a coverage of 9.5 μmole m^{-2} on copper has $T_c = 0.3$ K,[28] while on Vycor a similar coverage has $T_c = 0.5$ K.

In addition the low-temperature heat-capacity data for He on Ar-plated copper[27] can be fit by Eq. (1). However because the temperature regime covered did not extend to very low temperatures, no heat-capacity curves exhibited a break as seen in the present data. Also at coverages near 1 layer, the linear term in the heat capacity for ^{4}He on both copper and Ar-plated copper become very small,[26,29] behavior not observed for ^{4}He on Vycor. This behavior may be associated with the large variation in the isosteric heat of adsorption as a function of coverage seen at "monolayer" completion on heterogeneous substrates "smoother"[59] than Vycor.

Furthermore, our prediction that the ^{4}He film is undergoing a thermally activated increase in the number of atoms in free-particle states near the temperature T_c is substantiated by NMR spin-relaxation rate studies of ^{3} He films on Vycor.[60] (At low coverages, we expect the behavior of the film to be roughly independent of the adatom statistics since the behavior is substrate dominated). These spin-spin and spin-lattice relaxation experiments clearly indicated that at $T = 0.3$ K, a mobile-immobile transition of some form took place in the film at a coverage of about 14 μmole m^{-2}.[60] This observation correlates well with our observation that $T_c = 0.4$ K for a ^{4}He film of equivalent coverage.

TABLE IV. Parameters used to fit intermediate-coverage heat-capacity data using Eq. (1).

θ (Fractional filling)	A (10^4 erg K^{-2})	B (10^4 erg K^{-3})
0.319	4.65	3.03
0.348	5.35	4.01
0.363	6.34	4.72

We therefore conclude that the behavior of adsorbed helium films on any heterogeneous substrate in the low-coverage regime is substrate dominated and that the details of that behavior should yield information concerning the details of the substrate-helium interaction.

2. *Intermediate coverage films:* $0.319 \leq \theta \leq 0.397$

In Fig. 16 we plot the heat capacity (divided by T) for coverages in the vicinity of the critical coverage $\theta_0 = 0.337$ (28.6 μmole m^{-2}). As can be seen, for $T > T_0$ these films have heat capacities of the form $C = AT + BT^2$ just as do lower coverage films. (In Table IV we list the values of the parameter A and B for films). However, for $T < T_0$ the heat capacity of

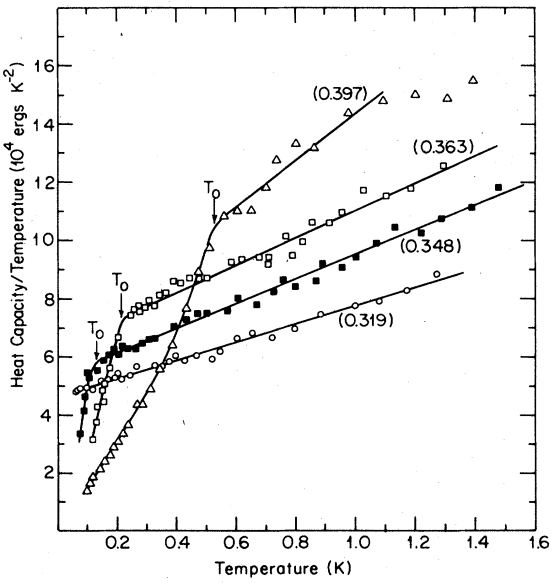

FIG. 16. Heat capacity divided by temperature for ^{4}He coverages near the critical coverage $\theta_0 = 0.337$ (28.6 μmole m^{-2}). Numbers in parentheses are coverages expressed as fractional filling.

these higher coverages falls dramatically. We associate the temperature T_0 with the onset of superfluidity for these films and assert that the break in the heat-capacity curves at this temperature is the remnant of the bulk λ anomaly. This assignment is based on the correspondence between the temperature T_0 and the temperature T_{onset} at which measured superflow begins. In Fig. 17 we plot T_0 (T_0 has been arbitrarily chosen as the temperature at which a smooth curve through the low-temperature data intersects a smooth curve through the high-temperature data) as a function of coverage along with the data for the coverage dependence of the cutoff temperature, T_c, which we discussed earlier. We have also included the measured onset temperatures (after properly scaling coverages) for superfluid flow for ^{4}He on Vycor glass seen by Berthold *et al.*[8] We note that every film that exhibits a break in the heat capacity at T_0 also exhibits a superfluid transition.[8] The heat-capacity feature at T_0 is the only anomaly in the heat-capacity data for films which are known to be superfluid at $T=0$.

The existence of a critical coverage in the neighborhood of 29 μmole m^{-2} has been noted in other studies of the properties of ^{4}He on glass. In particular the critical coverage $\theta_0=0.337$ (28.6 μmole m^{-2}) at which $T_0=T_{onset}=0$ is also the coverage for which Berthold *et al.*[8] observe the amount of ^{4}He participating in the superflow to go to 0. With the realization that a coverage of 29 μmole m^{-2} corresponds to a film thickness of about 1.5 standard atomic layers on glass (as discussed in Sec. III), we note that the results shown in Fig. 17 are comparable to the results of Scholtz *et al.*[30] who studied the onset of superfluidity (using third sound techniques) for ^{4}He films adsorbed on a glass slab. Scholtz *et al.* also noted that all the adsorbed ^{4}He for coverages greater than the critical coverage participate in superflow. Finally, recent thermodynamic calculations[37] on the properties of adsorbed helium films indicate that a coverage of about 29 μmole m^{-2} corresponds to the mass of solid helium that must be present on the surface of a glass substrate at low temperature before a liquid layer becomes thermodynamically allowed.

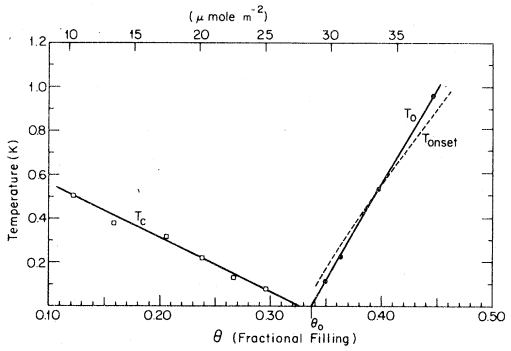

FIG. 17. Coverage dependence of T_0. Dashed lined labelled T_{onset} indicates the coverage dependence of the temperature for the onset of superfluidity on porous Vycor determined by Berthold *et al.* (Ref. 8).

All of these results support the following interpretation (which follows closely that of Chester *et al.*[37]) of the behavior of adsorbed ^{4}He films near critical. For coverages such that $\theta \leq \theta_0$ the film is all solid at $T=0$ while for $\theta > \theta_0$ the portion of the film θ_s above θ_0 ($\theta_s \equiv \theta - \theta_0$) is not bound to the solid at $T=0$ but exists as a superfluid layer on top of the solid. For $\theta > \theta_0$ our simple single-particle model predicts that the excess adatoms go into free-particle-like states with multiple occupancy (obeying Bose statistics) at all temperatures $T > 0$. However, since the form of the heat capacity of an ideal gas in two dimensions is independent of statistics (i.e., $C \propto T$) no change in the form of the heat capacity for $T > T_{onset}$ is expected when $\theta > \theta_0$. As long as the noninteracting single-particle picture is valid, we do not expect the form of the heat capacity to vary from the form $C = AT + BT^2$ until a superfluid transition takes place.

Considerable effort has been expended to determine whether or not superfluidity can really exist in two dimensions or only exists as a two-dimensional limit to three-dimensional superfluidity. While our data indicate that a superfluid transition does take place in films for which the mass of helium in the superfluid is quite small, the oscillating cavity experiments of Berthold *et al.*[8] have shown that the transition to superfluidity is three dimensional for ^{4}He on Vycor glass. The interconnected nature of the Vycor pore structure apparently leads to a three-dimensional character for the nature of the superfluid fluctuations with characteristic lengths greater than the pore diameter. Therefore, porous Vycor is not the substrate to use to answer questions concerning the existence of true two-dimensional superfluidity. Nevertheless, the excitation spectrum of superfluid ^{4}He confined in porous Vycor exhibits behavior that can be described in terms of a 2-D limit of the 3-D spectrum of He II. This behavior is discussed in Sec. IV A 3 of this paper.

3. *High-coverage films:* $\theta \geq 0.397$ (33.7 μmole m^{-2})

In Fig. 18 we show a representative set of heat-capacity curves for coverages in the high-coverage region. All of these films are superfluid at low temperatures and their heat capacities are determined in large measure by the nature of the elementary excitations in the superfluid. The form of the dispersion relation for elementary excitations in adsorbed superfluid ^{4}He films depends critically on whether or not a free surface (i.e. a gas-liquid interface) is present. Therefore we have broken our results down into two categories which we will discuss separately: (i) films

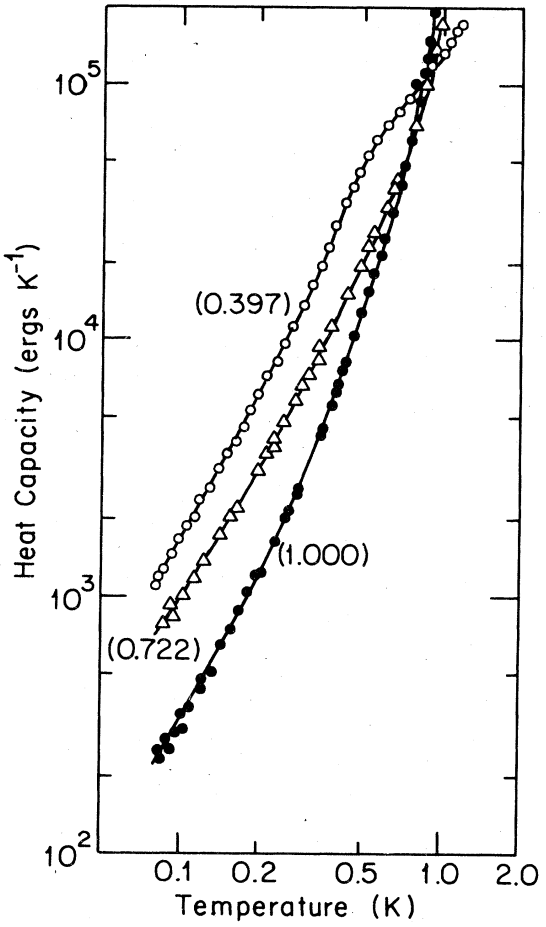

FIG. 18. Heat capacity of a representative set of ^{4}He coverages exhibiting superfluidity with $T_0 > 0.5$ K. Numbers in parentheses are coverages expressed as fractional filling. Solid lines are drawn as an aid to the eye.

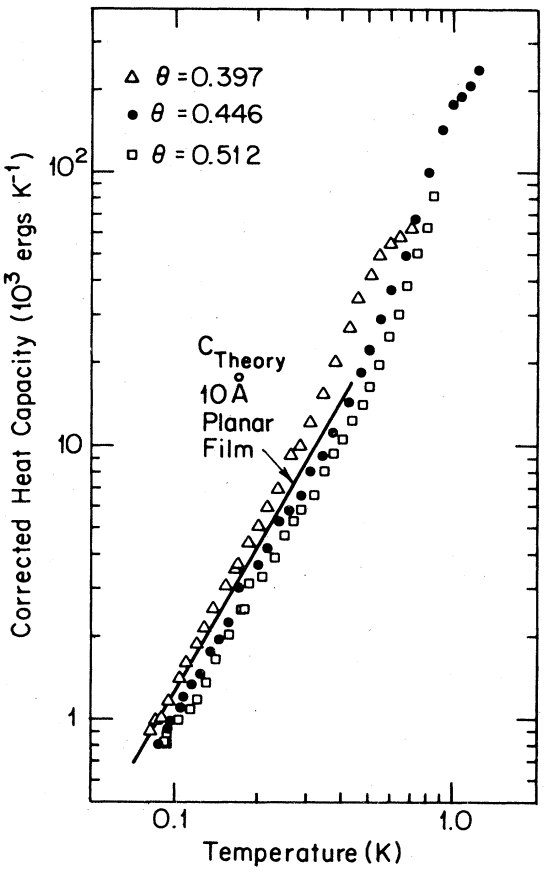

FIG. 19. Heat capacity of ^{4}He films having a free surface and exhibiting superfludity with $T_0 > 0.5$ K. The heat-capacity data plotted have been corrected for the heat capacity of the solid ^{4}He layer (see text for details). Numbers shown are coverages expressed as fractional filling. The solid line is the theoretical heat capacity of a planar superfluid ^{4}He film 10 Å thick (see Ref. 12).

having a gas-liquid interface and (ii) films having no gas-liquid interface (i.e., having full pores).

a. Films having a gas-liquid interface. In Figs. 19 and 20 we have plotted the low-temperature heat capacity of ^{4}He films that have superfluid onset temperatures $T_{onset} \geq 0.5$ K. The heat-capacity data shown for these films have been corrected for the T^2 contribution of the solid layer of helium at the surface of the Vycor by subtracting out a term $C_{solid} = (2.52 \times 10^4 \text{ erg/K}^{-3})\, T^2$ from each of the curves. This value for the solid layer contribution comes from an analysis of the full pore heat-capacity data we will discuss in Sec. IV A 3*b*. As can be seen, the heat-capacity curves for all the films at $T < 0.5$ K (the temperature at which we expect rotons to be effectively frozen out) have the form $C \propto T^{\delta}$ where δ varies smoothly from 1.85 to 1.66 as coverage increases. Also, it is obvious from the figures that the absolute magnitude of the helium heat capacity decreases smoothly as coverage increases and that there are no signs of any critical coverage effects.

Saam and Cole[12] have applied their quantum hydrodynamic methods to adsorbed superfluid films having a free surface and they found that the excitation spectrum at low temperatures was dominated by surface vibrational modes or ripplons. They found that the geometry of the free surface had a critical effects on these modes, and in particular they found that for superfluid films in cylindrical geometries the thermodynamic properties had interesting coverage dependent behavior. For a set of noninteracting cylindrical pores with a single pore radius they found that for thin superfluid films the heat capacity varied linearly with T at sufficiently low temperatures. They also found that as coverage increased the heat capaci-

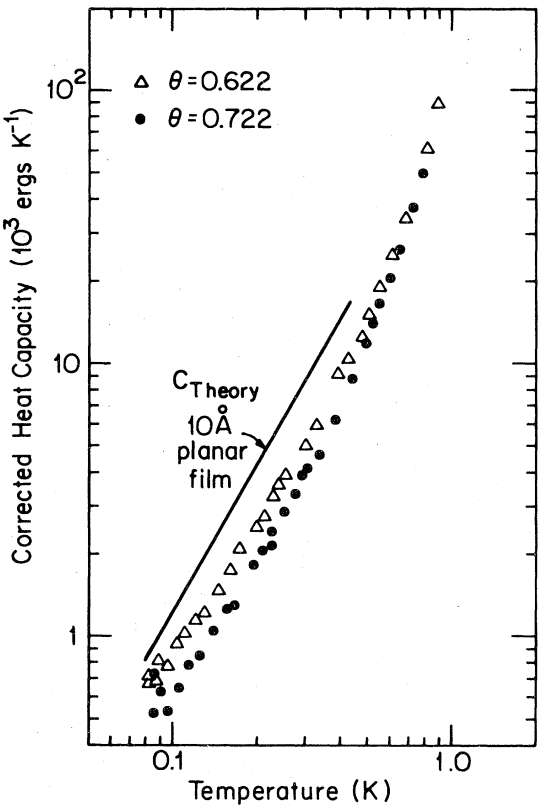

FIG. 20. Heat capacity of ^{4}He films having a free surface and exhibiting superfluidity with $T_{onset} > 1.5$ K. The heat-capacity data plotted have been corrected for the heat capacity of the solid ^{4}He layer (see text for details). The solid line is the theoretical heat capacity of a 10 Å planar film of superfluid ^{4}He (see Ref. 12 for details). Numbers shown are coverages expressed as fractional filling.

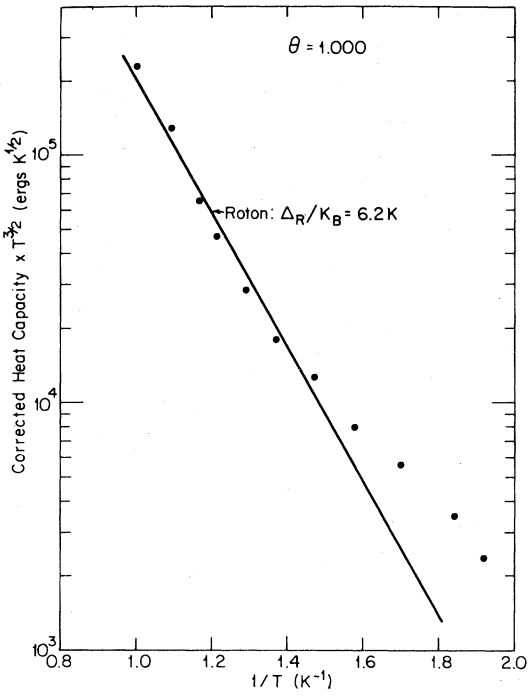

FIG. 21. High-temperature heat capacity of ^{4}He filling porous Vycor glass. The data have been plotted as $CT^{3/2}$ vs $1/T$ to indicate the portion of the heat-capacity data that can be fit by a roton heat capacity. The data have been corrected for the heat capacity of the solid ^{4}He layer (see text for details). The solid line is the form of the heat capacity for a roton term with energy gap $\Delta_R/k_B = 6.2$ K.

ty should increase. Furthermore they found that as a critical coverage ($\theta_c = 0.73$ for $R_p = 40$ Å) was approached the form of the low-temperature heat capacity should change and that it should then vary as $T^{1/2}$.

We do not observe the expected behavior for cylindrical geometry. In fact our results are consistent with the Saam and Cole predictions for *planar* geometry.[12] In Figs. 19 and 20 we have included the predicted heat capacity for a planar film 10 Å thick. (This thickness of ^{4}He on Vycor corresponds to about $\theta \sim 0.5$ for our sample). Both the absolute magnitude and the temperature dependence of the theoretical curve are in reasonable agreement with the experimental data. This planar behavior of superfluid films on Vycor is not really unexpected in light of the third sound results of Berthold *et al.*[8] These authors found that the observed variation of the velocity of third sound waves in Vycor could be quantitatively described by a planar model up to at least $\theta = 0.62$. Obviously the interconnected nature of the pores in porous Vycor glass leads to an effective planar density of states for the ripplon modes.

The observed decrease in the absolute magnitude of the heat capacity as coverage increased is contrary to the expected dependence for planar films. An increase in film thickness leads to a decrease in the velocity of third sound waves and hence should lead to an increased film heat capacity. However, as we pointed out earlier, there is a distribution of different pore radii in porous Vycor and the decrease in heat capacity that we observe is probably due to a filling up of the smaller pores (due to capillary condensation) and the consequent decrease in the amount of free surface.

b. Full Pores: $\theta = 1.000$. The heat capacity of ^{4}He filling the pores of our sample of porous Vycor is shown in Fig. 18. This coverage is known to have a superfluid onset at $T_{onset} \approx 2.0$ K.[5,11] Therefore we know that for $T \leq 1.0$ K there are essentially no residual effects of the transition on the form of the heat capacity and we can describe the heat capacity in terms of the elementary excitations of the system.

For $T \gtrsim 0.6$ K the observed heat capacity can be accounted for by a roton-type term of the form $C = BT^{-3/2}e^{-\Delta_R/k_BT}$. Here B is a constant and Δ_R is the roton energy gap. In Fig. 21 we have plotted

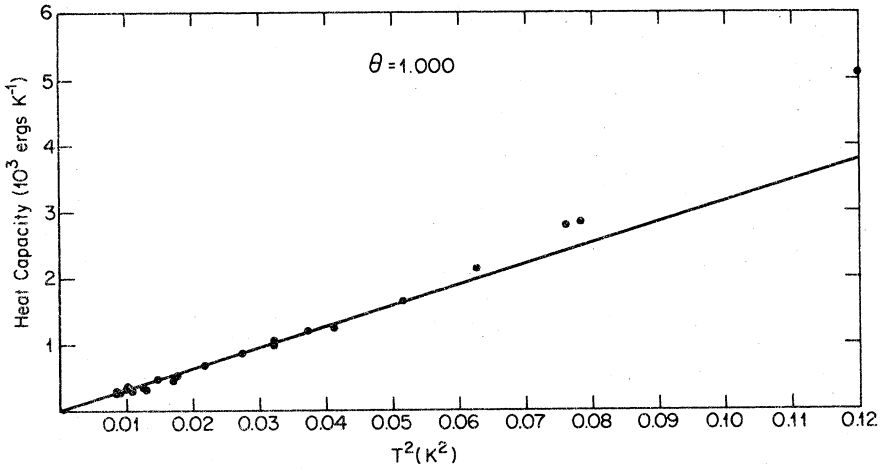

FIG. 22. Low-temperature heat capacity of ^{4}He filling porous Vycor. The data have been plotted as $C(T)$ vs T^2 to emphasize the T^2 temperature dependence of the data for $T < 0.25$ K.

$CT^{3/2}$ (after correcting for the heat capacity of the solid layer of ^{4}He at the Vycor surface) versus T^{-1} to demonstrate this fact. The data can be well fit using the value $\Delta_R/k_B = 6.2$ K. This value for the roton gap is in excellent agreement with the value of 6.1 K used by Brewer *et al.*[9] to describe the roton portion of the heat capacity for filled pores on their sample of porous Vycor. Also, this value for Δ_R compares well with the value $\Delta_R/k_B = 5.85$ K found by Kiewiett *et al.*[11] to describe the roton contribution to the normal fluid density of ^{4}He filling porous Vycor. The observed reduction of the roton gap of about 2.5 K below the bulk value of $\Delta_R/k_B = 8.7$ K is consistent with Padmore's Feynman-Cohen-type calculations[49] in which he found that 2-D rotons should have an energy gap about 1.9 K lower than 3-D rotons.

The full pore heat-capacity data in the temperature range $T \lesssim 0.6$ K is not as readily characterized in terms of superfluid excitations as was the heat-capacity data in the same temperature range for films with a free surface because of the obscuring effect of the solid layer heat capacity. For the films with a free surface, the ripplon contribution to the heat capacity was typically 70% or more of the total heat capacity so that uncertainties in the heat capacity of the solid layer would not significantly alter any of the corrected heat-capacity curves. However, for full pores, the solid layer seems to account for 80% or more of the observed heat capacity for $T < 0.3$ K and on the order of 50% for $0.3 < T < 0.5$ K. Therefore, for full pores a small change in the choice of a solid layer heat capacity has a large effect on the magnitude of the residual heat capacity which we attribute to superfluid excitation.

In Fig. 22 we plot the heat capacity of full pores as a function of T^2. As can be seen, the data for $T < 0.25$ K can be well fit by an equation $C = BT^2$ where $B = 3.15 \times 10^4$ erg K^{-2}. If we assume that this

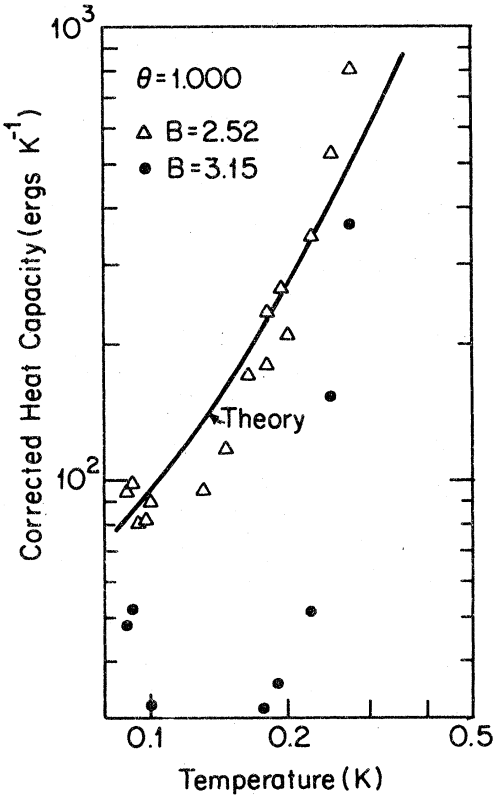

FIG. 23. Low-temperature heat capacity of ^{4}He filling porous Vycor corrected using different values for the solid layer heat capacity. Δ: data corrected using $C_s = 2.52T^2 \times 10^4$ erg K^{-3}; •: data corrected using $C_s = 3.15T^2 \times 10^4$ erg K^{-3}. Solid line is the theoretical heat capacity of superfluid ^{4}He filling nonintersecting channels 70 Å in diameter (see text).

T^2 term is the contribution of the two-dimensional solid then we find that the excess heat capacity for $T < 0.28$ K is small. However, if we assume that the solid layer contribution is 20% smaller (i.e., $B = 2.52 \times 10^4$ erg K^{-2}) then we find that the excess heat capacity is substantial. In Fig. 23 we show the excess heat capacity obtained using these two different values for the solid layer correction.

Saam and Cole[12] have calculated the heat capacity of superfluid ^{4}He filling a collection of nonintersecting pores. The calculated low-energy excitation spectrum for the system was found to be composed of phonon modes having a velocity of sound equal to the bulk sound velocity and satisfying the proper boundary conditions for cylindrical geometry. In Fig. 23 we have also plotted the Saam and Cole[12,60] prediction for the heat capacity of ^{4}He filling pores having a radius $R = 34$ Å (we have subtracted out the 5 Å solid layer).

As can be seen, the experimental data corrected using the smaller value for the solid heat-capacity contribution looks substantially more like the theoretical curve than the data corrected using the larger value for this correction. Since fourth sound measurements[11] have indicated that there are indeed a substantial number of superfluid excitations for superfluid ^{4}He filling porous Vycor in this temperature range we expect that the lower value for the solid layer correction is closer to the truth. (Therefore we used a term $C = BT^2$ with $B = 2.5 \times 10^4$ erg K^{-2} to correct our earlier free surface data).

However, because we have no direct experimental or theoretical justification for choosing a particular expression to correct for the solid layer heat capacity, we conclude that our data is not sufficient at present to check the validity of the Saam and Cole model.[12] In particular, if porous Vycor data is to be used as a test of this model then one of two things are needed: (i) an accurate value for the solid layer heat capacity or (ii) heat-capacity data below $T = 0.08$ K where the solid layer term should be small.

B. N_2-plated Vycor

Examination of the heat-capacity data for ^{4}He films adsorbed on porous Vycor glass preplated with a BET monolayer of N_2 shows that the behavior of these films is essentially identical to that of ^{4}He films on bare Vycor except that the weaker adsorption potential of the N_2-covered surface shifts the coverage dependence of all behavior of these films to lower coverages. In Fig. 24 we show the total ^{4}He heat capacity at $T = 0.1$ K as a function of coverage for ^{4}He on both bare Vycor and N_2-preplated Vycor.[61] As can be seen, there is a shift of about 0.25×10^{-2} mole (8 μmole m^{-2}) from the bare to the preplated substrate. This decrease is consistent with the expected

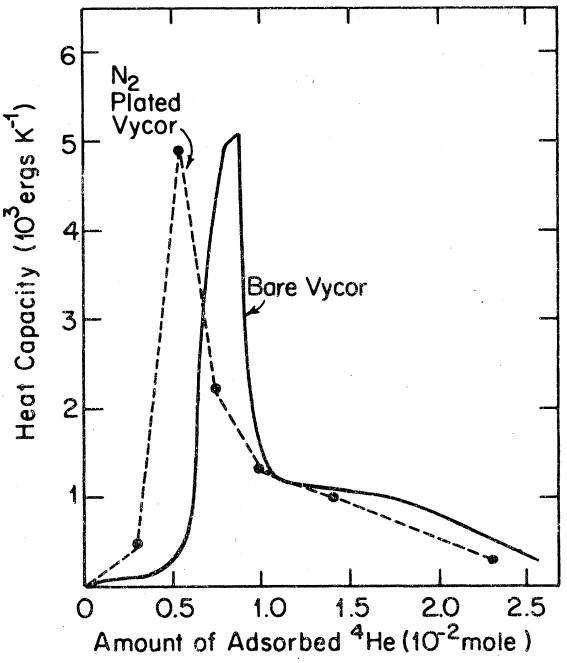

FIG. 24. ^{4}He heat capacity as a function of coverage (at $T = 0.1$ K) for ^{4}He adsorbed on N_2-preplated Vycor. Solid line is the data for ^{4}He adsorbed on bare Vycor. Note the shift in the peak location by about 0.25×10^2 mole (8 μmole m^{-2}).

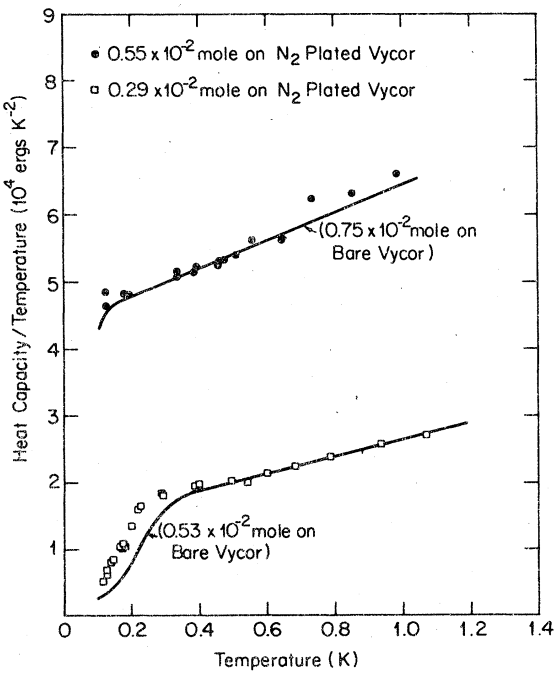

FIG. 25. Heat capacity divided by temperature for low-coverage ^{4}He films on N^2-preplated Vycor compared with previous data for comparable ^{4}He films on bare Vycor.

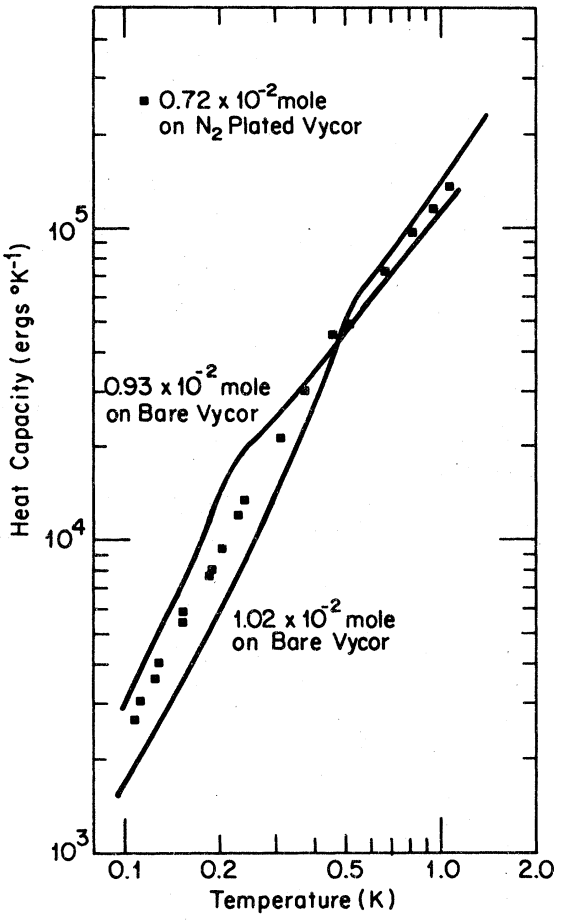

FIG. 26. Heat capacity of intermediate-coverage ^{4}He film on N_2-preplated Vycor compared with previous data for comparable ^{4}He films on bare Vycor.

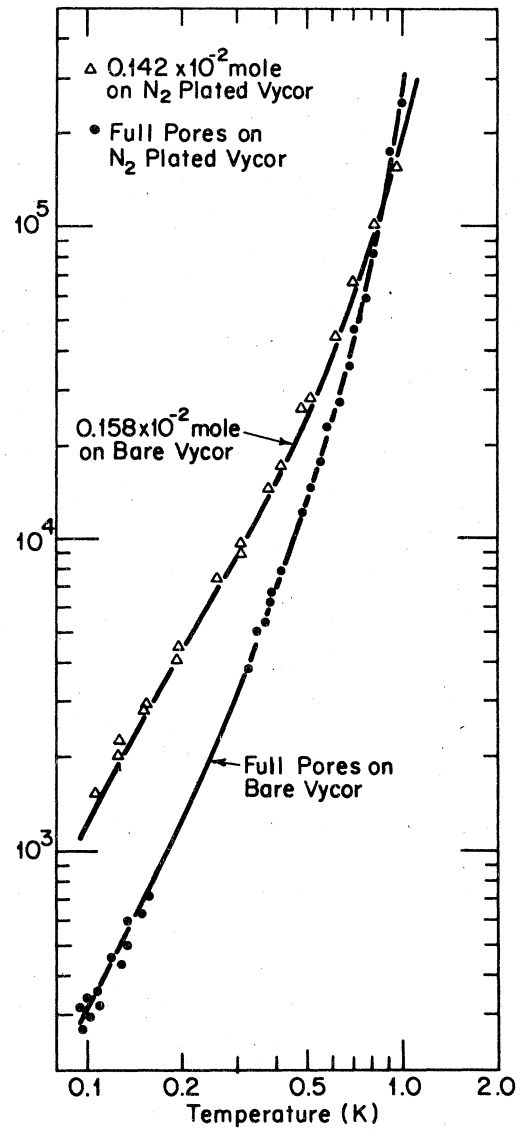

FIG. 27. Heat capacity of high-coverage ^{4}He films on N_2-preplated Vycor compared with previous data for comparable ^{4}He films on bare Vycor.

lowering and smoothing of the effective Van der Waals attraction between the adsorbed helium and the substrate due to the presence of the N_2, and it is consistent with the consequent lowering in the amount of ^{4}He required to form the solid helium layer at the Vycor surface.

Further evidence for the equivalence of the behavior of ^{4}He films adsorbed on bare Vycor and N_2-preplated Vycor is given in Figs. 25–27. In these figures we have plotted the heat capacity of ^{4}He films adsorbed on coated Vycor along with the heat capacity of films on bare Vycor that we expect to have equivalent behavior. It is obvious from the figures that the form of the heat-capacity curves for these two substrates are essentially identical once the coverage shift has been considered.

We argue that all of the mechanisms that we have used to describe the behavior of ^{4}He adsorbed on bare Vycor are now directly applicable to ^{4}He adsorbed on coated Vycor. Therefore it seems apparent that the details of the form of the adsorption potential for heterogeneous substrates does not play a determining role in the general behavior of the adsorbed helium film but only effects the numerical values of the relevant parameters.

V. SUMMARY AND CONCLUSIONS

We summarize our conclusions about the low-temperature form of adsorbed ^{4}He on bare Vycor glass in the phase diagram shown in Fig. 28. We

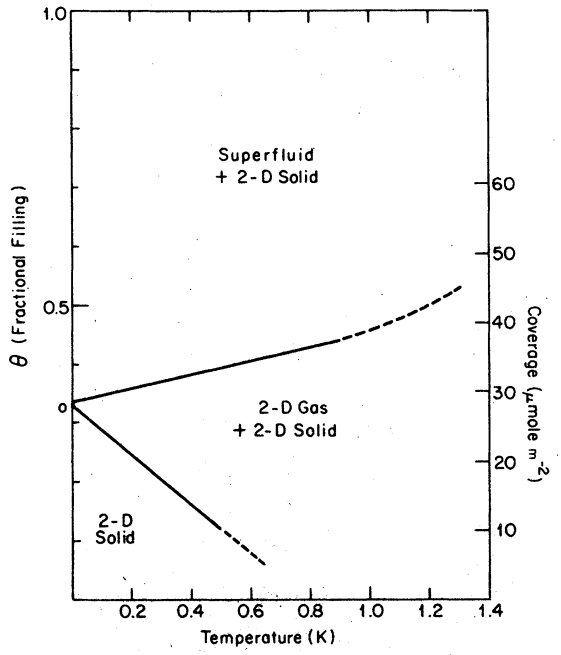

FIG. 28. Proposed phase diagram for ^{4}He films on porous Vycor glass.

have concluded that the heat capacity of the phases shown can be explained in terms of the following elementary excitations within these phases: (i) 2-D pseudo-Debye phonons in the 2-D solid, (ii) single-particle excitations plus 2-D pseudo-Debye phonons in the combined 2-D gas and 2-D solid phase and (iii) superfluid excitations plus 2-D pseudo-Debye phonons in the combined superfluid and 2-D solid phase. Finally we conclude that a similar phase diagram and a similar excitation spectrum are probably characteristic of adsorbed ^{4}He on all heterogeneous substrates.

ACKNOWLEDGMENTS

We gratefully thank R. O. Pohl for his help and encouragement. This work was supported by the U.S. AEC under Contract No. AT(11-1)-3151; by the NSF under Grant No. GH-37658; by the NSF under Grant No. GH-33637, through the Cornell Materials Science Center, Technical Report No. 3090.

APPENDIX A

In this Appendix we give the derivation of the heat capacity of the simple single-particle system containing N_0 noninteracting particles with the band structure shown in Fig. 14. We require that the levels for $E \leq E_0$ have only single occupancy while states with $E \geq E_0 + 2\Delta$ have multiple occupancy. We have N_0 atoms adsorbed. With the constant density of states G_0 we have

$$N_0 = \int_0^{E_0} G_0 \, d\epsilon = G_0 E_0 \ . \tag{A1}$$

We also assume that $G_0 \sim H_0$ and $E_0 >> \Delta$.

For temperature T we then have

$$N_0 = \int_0^{E_0} G_0 \frac{d\epsilon}{e^{\beta(\epsilon-\mu)}+1} + \int_{E_0+2\Delta}^{\infty} H_0 \frac{d\epsilon}{e^{\beta(\epsilon-\mu)}-1} \tag{A2}$$

or

$$N_0 = \int_0^{E_0} G_0 \, d\epsilon - \int_0^{E_0} G_0 \frac{e^{\beta(\epsilon-\mu)} \, d\epsilon}{e^{\beta(\epsilon-\mu)}+1} + \int_{E_0+2\Delta}^{\infty} H_0 \frac{d\epsilon}{e^{\beta(\epsilon-\mu)}-1} \ . \tag{A3}$$

Here $\beta = 1/k_B T$ and μ is the chemical potential.

We also have that the total energy of the system E is given by

$$E = \int_0^{E_0} G_0 \frac{\epsilon}{e^{\beta(\epsilon-\mu)}+1} \, d\epsilon + \int_{E_0+2\Delta}^{\infty} H_0 \frac{\epsilon}{e^{\beta(\epsilon-\mu)}-1} \, d\epsilon \tag{A4}$$

or

$$E = \int_0^{E_0} G_0 \epsilon \, d\epsilon - \int_0^{E_0} G_0 \frac{\epsilon \, e^{\beta(\epsilon-\mu)}}{e^{\beta(\epsilon-\mu)}+1} \, d\epsilon + \int_{E_0+2\Delta}^{\infty} H_0 \frac{\epsilon}{e^{\beta(\epsilon-\mu)}-1} \, d\epsilon \ . \tag{A5}$$

Now let us examine the behavior for $\Delta >> k_B T$. In this case we have $\beta(\epsilon-\mu) >> 1$ for $\epsilon > E_0 + 2\Delta$ and we also have $\beta(\mu-\epsilon) >> 1$ for $\epsilon < E_0$ since (as we will show) $\mu \sim E_0 + \Delta$.

We therefore have $\epsilon^{\beta(\epsilon-\mu)} >> 1$ for $\epsilon > E_0 + 2\Delta$ and $\epsilon^{\beta(\epsilon-\mu)} << 1$ for $\epsilon < E_0$. Therefore we find

$$N_0 \approx G_0 E_0 - \int_0^{E_0} G_0 \, e^{-\beta(\epsilon-\mu)} \, d\epsilon + \int_{E_0+2\Delta}^{\infty} H_0 \, e^{-\beta(\epsilon-\mu)} \, d\epsilon \ . \tag{A6}$$

Carrying out the integration we have

$$0 = \frac{G_0 e^{-\beta(\mu)}}{\beta} - \frac{G_0}{\beta} e^{\beta(E_0-\mu)} + \frac{H_0}{\beta} e^{-\beta(E_0+2\Delta-\mu)} \ . \tag{A7}$$

Noting that $e^{-\beta\mu} << e^{\beta(E_0-\mu)}$ we get

$$G_0 e^{\beta(E_0-\mu)} \approx H_0 e^{-\beta(E_0+2\Delta-\mu)} \ .$$

Therefore we have (to lowest order in $k_B T$)

$$\mu = E_0 + \Delta + k_B T \ln(G_0/H_0)^{1/2} \tag{A8}$$

Using the assumption that $k_BT << \Delta$ and Eq. (A5) we have

$$E = \tfrac{1}{2}G_0E_0^2 - G_0\int_0^{E_0} \epsilon\, e^{\beta(\epsilon-\mu)}\, d\epsilon + H_0\int_{E_0+2\Delta}^{\infty} \epsilon\, e^{-\beta(\epsilon-\mu)}\, d\epsilon \ . \tag{A9}$$

Carrying out the integration we find

$$E = \tfrac{1}{2}G_0E_0^2 - G_0e^{-\beta\mu}\left(\frac{E_0e^{\beta E_0}}{\beta} - \frac{e^{\beta E_0}}{\beta^2} - \frac{1}{\beta^2}\right) + H_0e^{\beta\mu}\left(\frac{(E_0+2\Delta)e^{-\beta(E_0+2\Delta)}}{\beta^2} - \frac{e^{-\beta(E_0+2\Delta)}}{\beta^2}\right) . \tag{A10}$$

Using Eq. (A7) for μ we find

$$E = \tfrac{1}{2}G_0E_0^2 - \frac{G_0E_0}{\beta}\left(\frac{H_0}{G_0}\right)^{1/2}e^{-\beta\Delta} + \frac{G_0}{\beta^2}\left(\frac{B_0}{A_0}\right)^{1/2}e^{-\beta\Delta} + \frac{G_0}{\beta^2}e^{-\beta(E_0+\Delta)} + \frac{H_0}{\beta}(E_0+2\Delta)\left(\frac{G_0}{H_0}\right)^{1/2}e^{-\beta\Delta} - \frac{G_0}{\beta^2}\left(\frac{G_0}{H_0}\right)^{1/2}e^{-\beta\Delta} \ . \tag{A11}$$

Therefore we get

$$E = \tfrac{1}{2}G_0E_0^2 + \frac{2\Delta}{\beta}(G_0H_0)^{1/2}e^{-\beta\Delta} + \frac{G_0}{\beta^2}e^{-\beta\Delta} + \frac{G_0}{\beta^2}e^{-\beta E_0}e^{-\beta\Delta} \ . \tag{A12}$$

Again noting that $e^{-\beta E_0}/\beta << 2\Delta$ we have

$$E \approx \tfrac{1}{2}G_0E_0^2 + \frac{2\Delta}{\beta}(G_0H_0)e^{-\beta\Delta} \ . \tag{A13}$$

Now $C = \partial E/\partial T$ so that (to lowest orders in Δ/k_BT) we find

$$C = 2(G_0H_0)^{1/2}e^{-\beta\Delta}\Delta k_B\left(\frac{\Delta}{k_BT}+2\right); \quad \Delta/k_BT >> 1 \ . \tag{A14}$$

Now we will calculate the chemical potential and heat capacity in the limit $\Delta/k_BT << 1$. To do this we will simply set $\Delta \equiv 0$. To begin we again write

$$N_0 = \int_0^{E_0} G_0\, d\epsilon = G_0E_0 \ .$$

For $T > 0$ and $\Delta = 0$ we have

$$N_0 = \int_0^{E_0} G_0\frac{d\epsilon}{e^{\beta(\epsilon-\mu)}+1} + \int_{E_0}^{\infty} H_0\frac{d\epsilon}{e^{\beta(\epsilon-\mu)}-1} \ , \tag{A15}$$

or

$$N_0 = \int_0^{E_0} G_0\, d\epsilon - \int_0^{E_0} G_0\frac{e^{\beta(\epsilon-\mu)}}{e^{\beta(\epsilon-\mu)}+1}\, d\epsilon + \int_{E_0}^{\infty}\frac{H_0}{e^{\beta(\epsilon-\mu)}-1}\, d\epsilon \ , \tag{A16}$$

$$N_0 = N_0 - \int_{-E_0}^{0} G_0\frac{e^{\beta(\epsilon+E_0-\mu)}}{e^{\beta(\epsilon+E_0-\mu)}+1}\, d\epsilon + \int_0^{\infty}\frac{H_0}{e^{\beta(\epsilon+E_0-\mu)}-1} \ . \tag{A17}$$

Noting that for the last integral to be finite we must have $E_0 - \mu > 0$ we set $\mu = E_0 - \xi$ and realize that $\xi > 0$.

Setting $e^{\beta\xi} \equiv a$ we get

$$\int_{-E_0}^{0} G_0\frac{ae^{\beta\epsilon}}{ae^{\beta\epsilon}+1}\, d\epsilon = \int_0^{\infty}\frac{H_0}{ae^{\beta}-1}\, d\epsilon \ . \tag{A18}$$

We also note that since $\beta E_0 >> 1$ we can change the lower limit of integration for the integral on the left from $-E_0$ to $-\infty$ without changing the value of the integral appreciably.

Therefore

$$\int_{-\infty}^{0} G_0\frac{ae^{\beta\epsilon}}{ae^{\beta\epsilon}+1}\, d\epsilon = \int_0^{\infty} H_0\frac{1}{ae^{\beta\epsilon}-1}\, d\epsilon \ . \tag{A19}$$

Carrying out the integration we get

$$\frac{G_0}{\beta}\ln(a+1) = \frac{H_0}{\beta}\ln\left(\frac{a}{a-1}\right) \ . \tag{A20}$$

If we set $Q = e^{G_0/H_0}$, then

$$Qa^2 - a - Q = 0 \ . \tag{A21}$$

Solving this quadratic equation we find that a is independent of β; i.e.,

$$a = \frac{1+(1+4Q^2)^{1/2}}{2Q} \ . \tag{A22}$$

To calculate the heat capacity we first write that

$$E = \int_0^{E_0} G_0\frac{\epsilon}{e^{\beta(\epsilon-\mu)}+1}\, d\epsilon + \int_{E_0}^{\infty} H_0\frac{\epsilon}{e^{\beta(\epsilon-\mu)}-1}\, d\epsilon \tag{A23}$$

or

$$E = \int_0^{E_0} G_0\epsilon\, d\epsilon - \int_0^{E_0} H_0\frac{\epsilon e^{\beta(\epsilon-\mu)}}{e^{\beta(\epsilon-\mu)}+1}\, d\epsilon + \int_{E_0}^{\infty} H_0\frac{\epsilon}{e^{\beta(\epsilon-\mu)}-1}\, d\epsilon \ . \tag{A24}$$

Noting that $e^{-\beta\mu} = e^{-\beta(F_0-\xi)}$ we have

$$E = \tfrac{1}{2}G_0E_0^2 - \int_{-E_0}^{0} G_0 \frac{(\epsilon+E_0)e^{\beta\xi}e^{\beta\epsilon}}{e^{\beta\xi}e^{\beta\epsilon}+1}\,d\epsilon + \int_0^\infty H_0 \frac{\epsilon+E_0}{e^{\beta\xi}e^{\beta\epsilon}-1}\,d\epsilon \ . \tag{A25}$$

Recalling Eq. (A18) and the fact that $A = e^{\beta\xi}$ we get

$$E = \tfrac{1}{2}G_0E_0^2 - \int_{-E_0}^{0} G_0 \frac{\epsilon a e^{\beta\epsilon}}{ae^{\beta\epsilon}+1}\,d\epsilon + \int_0^\infty H_0 \frac{\epsilon}{ae^{\beta\epsilon}-1}\,d\epsilon \ . \tag{A26}$$

Noting that $\beta E_0 >> 1$ we see that the lower limit in the first integral on the right side of Eq. (A26) can be set equal to $-\infty$ without significantly affecting the integral. Setting $x = \beta\epsilon$ we get

$$E = \tfrac{1}{2}G_0E_0^2 - \frac{G_0}{\beta^2}\int_{-\infty}^{0} \frac{axe^x}{ae^x+1}\,dx + \frac{H_0}{\beta^2}\int_0^\infty H_0 \frac{x}{ae^x-1}\,dx \ , \tag{A27}$$

or

$$E = \tfrac{1}{2}G_0E_0^2 + G_0(k_BT)^2\int_0^\infty \frac{axe^{-x}}{ae^{-x}+1}\,dx + H_0(k_BT)^2\int_0^\infty \frac{x}{ae^x-1}\,dx \ . \tag{A28}$$

Therefore

$$C = \frac{\partial E}{\partial T} = \left[G_0k_B^2\int_0^\infty \frac{axe^{-x}}{ae^{-x}+1}\,dx + H_0k_B^2\int_0^\infty \frac{x}{ae^x-1}\,dx\right]T \tag{A29}$$

or

$$C = (G_0K_1k_B^2 + H_0K_2k_B^2)\,T, \quad \Delta/k_BT << 1 \ . \tag{A30}$$

Here

$$K_1\int_0^\infty \frac{axe^{-x}}{ae^{-x}+1}\,dx$$

and

$$K_2 = \int_0^\infty \frac{x}{ae^x-1}\,dx \ .$$

We can evaluate these integrals numerically for a given value of a. For $a = 1.50$ we find

$$K_1 = 1.15, \quad K_2 = 0.83 \ .$$

---

*Present address: Central Research and Development Dept., E. I. duPont deNemours and Co., Wilmington, Del. 19898.

[1] F. D. Manchester, Rev. Mod. Phys. 39, 383 (1967).
[2] D. F. Brewer, J. Low Temp. Phys. 3, 205 (1970).
[3] M. Bretz, J. G. Dash, D. C. Hickernell, E. O. McLean, and O. E. Vilches, Phys. Rev. A 8, 1589 (1973).
[4] R. L. Eigin and D. L. Goodstein, Phys. Rev. A 9, 2657 (1974).
[5] D. Brewer, in *The Physics of Liquid and Solid Helium,* edited by K. H. Bennemann and J. B. Ketterson (Wiley, New York 1978), part 2.
[6] A. Eggington, in *The Helium Liquids,* edited by J. Armitage and I. Farquhar (Academic, New York, 1975).
[7] J. G. Dash, Phys. Rev. B 15, 313 (1977); B. A. Huberman and J. G. Dash, Phys. Rev. B 17, 398 (1978).
[8] J. E. Berthold, D. J. Bishop, and J. D. Reppy, Phys. Rev. Lett. 39, 348 (1977).
[9] D. F. Brewer, A. J. Symonds, and A. L. Thompson, Phys. Rev. Lett. 15, 182 (1965).
[10] F. D. M. Pobell, H. W. Chan, L. R. Corrucini, R. P. Henkel, S. W. Schwenterly, and J. D. Reppy, Phys. Rev. Lett. 28, 542 (1972).
[11] C. W. Kiewet, H. E. Hall, and J. D. Reppy, Phys. Rev. Lett. 35, 1286 (1975).
[12] W. F. Saam and M. W. Cole, Phys. Rev. B 11, 1086 (1975).
[13] D. E. Hagen, A. D. Novaco, and F. J. Milford, in *Proceedings of the Second International Symposium on Adsorption-Desorption Phenomena, Florence* (Academic, New York, 1971).
[14] E. Giamello, C. Pisani, F. Ricca, and C. Roetti, Surf. Sci. 49, 401 (1975).
[15] F. J. Milford and A. D. Novaco, Phys. Rev. A 4, 1136 (1971).
[16] A. D. Novaco and F. J. Milford, Phys. Rev. A 5, 783 (1972).
[17] A. D. Novaco, Phys. Rev. B 15, 5217 (1977).
[18] J. E. Lennard-Jones and A. F. Devonshire, Proc. R. Soc. London Sect. A 158, 242 (1937), 158, 253 (1937).
[19] G. G. Kleiman and V. Landman, Phys. Rev. Lett. 31, 707 (1973); G. G. Kleiman and U. Landman, Phys. Rev. B 8, 5484 (1973).
[20] F. J. Milford, in *Monolayer and Submonolayer Helium Films,* edited by J. G. Daunt and E. Lerner (Plenum, New York, 1973).
[21] A. D. Novaco and F. J. Milford, J. Low Temp. Phys. 3, 307 (1970).
[22] A. D. Novaco and C. E. Campbell, Phys. Rev. B 11, 2525 (1975).
[23] R. L. Siddon and M. Schick, Phys. Rev. A 9, 907 (1974).
[24] B. F. Cowan, M. G. Richards, A. L. Thomson, and W. J. Mullin, Phys. Rev. Lett. 38, 165 (1977).
[25] K. Carneiro, W. D. Ellenson, L. Passell, J. P. McTague, and H. Taulo, Phys. Rev. Lett. 37, 1695 (1976).
[26] W. D. McCormick, D. L. Goodstein, and J. G. Dash, Phys. Rev. 168, 249 (1968).
[27] G. A. Stewart and J. G. Dash, Phys. Rev. A 2, 918 (1970).
[28] D. C. Hickernell, E. O. McLean, and O. E. Vilches, J. Low. Temp. Phys. 13, 241 (1973).
[29] N. N. Roy and G. D. Halsey, J. Low Temp. Phys. 4, 231 (1971).

[30]J. H. Scholtz, E. O. McLean, and I. Rudnick, Phys. Rev. Lett. 32, 147 (1974).
[31]T. E. Washburn, J. E. Rutlege, and J. M. Mochel, Phys. Rev. Lett. 34, 183 (1975).
[32]M. H. W. Chan, A. W. Yanoff, and J. D. Reppy, Phys. Rev. Lett. 32, 1347 (1974).
[33]J. A. Herb and J. G. Dash, Phys. Rev. Lett. 29, 846 (1972).
[34]E. S. Sabisky and C. H. Anderson, Phys. Rev. Lett. 30, 1122 (1973).
[35]M. Chester and L. C. Yang, Phys. Rev. Lett. 31, 1377 (1973).
[36]J. A. Herb and J. G. Dash, Phys. Rev. Lett. 35, 171 (1975).
[37]M. Chester and L. Eytel, Phys. Rev. B 13, 1069 (1976).
[38]V. L. Ginzburg and L. P. Pitaevskii, Zh. Eksp. Teor. Fiz. 34, 1240 (1958) [Sov. Phys. JETP 7, 858 (1958)].
[39]S. Doniach, Phys. Rev. Lett. 31, 1450 (1973).
[40]J. G. Dash, Phys. Rev. B 15, 3136 (1977).
[41]B. A. Huberman and J. G. Dash, Phys. Rev. B 17, 398 (1978).
[42]J. M. Kosterlitz and D. J. Thouless, J. Phys. C 6, 1181 (1973); B. A. Huberman, R. J. Myerson, and S. Doniach, Phys. Rev. Lett. 40, 780 (1978); V. Ambegaokar, B. I. Halperin, D. R. Nelson, and E. D. Siggia, Phys. Rev. Lett. 40, 783 (1978).
[43]I. Rudnick, Phys. Rev. Lett. 40, 1454 (1978).
[44]D. J. Bishop and J. D. Reppy, Phys. Rev. Lett. 40, 1727 (1978).
[45]S. Gregory and C. C. Lim, Phys. Rev. A 9, 2252 (1974).
[46]J. R. Clow and J. D. Reppy, Phys. Rev. A 5, 424 (1972).
[47]M. Bretz, Phys. Rev. Lett. 31, 1447 (1973).
[48]T. C. Padmore, Phys. Rev. Lett. 28, 1512 (1972).
[49]T. C. Padmore, Phys. Rev. Lett. 32, 826 (1974).
[50]S. Scholes and F. C. F. Wilkinson, Faraday Soc. Discuss. 50, 175 (1970); J. H. P. Watson, Phys. Rev. 148, 223 (1966); J. H. P. Watson, Phys. Rev. B 2, 1282 (1970).
[51]S. J. Gregg and K. S. W. Sing, *Adsorption, Surface Area, and Porosity* (Academic, New York, 1967).
[52]M. H. W. Chan, Ph.D. thesis (Cornell University, 1974) (unpublished).
[53]J. E. Berthold (private communication).
[54]A. J. Symonds, Ph.D. thesis (University of Susses, 1965) (unpublished).
[55]E. S. Sabisky and C. H. Anderson, Phys. Rev. A 7, 790 (1973).
[56]J. G. Daunt, Phys. Lett. A 41, 223 (1972).
[57]W. A. Steele and J. G. Aston, J. Amer. Chem. Soc. 79, 2393 (1957).
[58]J. G. Daunt and E. Lerner, J. Low Temp. Phys. 8, 79 (1972).
[59]D. F. Brewer, D. J. Cresswell, Y. Goto, M. G. Richards, J. Rolt, and A. L. Thomson, in *Monolayer and Submonolayer Helium Films*, edited by J. G. Daunt and E. Lerner (Plenum, New York, 1973).
[60]Theoretical heat capacity for $T > 0.1$ K was calculated using the ten largest terms in the total energy sum [Eq. (3.6) in Ref. 12] and evaluating the integral over K [Eq. (3.9) in Ref. 12] numerically.
[61]Specific surface coverages for ^{4}He on N_2-preplated Vycor shown in Fig. 24 have been corrected for the approximate 7% loss of surface area that arose from the slight filling of cylindrical pores by the adsorbed N_2.